

Quantification and microstructural origin of the anisotropic nature of the sensitivity to brittle cleavage fracture propagation for hot-rolled pipeline steels

F. Tankoua · J. Crépin · P. Thibaux ·
S. Cooreman · A.-F. Gourgues-Lorenzon 

Received: 14 November 2017 / Accepted: 22 June 2018 / Published online: 29 June 2018
© Springer Nature B.V. 2018

Abstract This work proposes a quantitative relationship between the resistance of hot-rolled steels to brittle cleavage fracture and typical microstructural features, such as microtexture. More specifically, two hot-rolled ferritic pipeline steels were studied using impact toughness and specific quasistatic tensile tests. In drop weight tear tests, both steels exhibited brittle out-of-plane fracture by delamination and by so-called “abnormal” slant fracture, here denoted as “brittle tilted fracture” (BTF). Their sensitivity to cleavage cracking was thoroughly determined in the fully brittle temperature range using round notched bars, according to the local approach to fracture, taking anisotropic plastic flow into account. Despite limited anisotropy in global texture and grain morphology, a strong anisotropy in critical cleavage fracture stress was evidenced for the two steels, and related through a Griffith-inspired approach to the size distribution of clusters of unfavorably oriented ferrite grains (so-called “potential cleavage facets”). It was quantitatively demonstrated that the occurrence

of BTF, as well as the sensitivity to delamination by cleavage fracture, is primarily related to an intrinsically high sensitivity of the corresponding planes to cleavage crack propagation across potential cleavage facets.

Keywords Ferritic steels · Brittle cleavage fracture · Impact toughness · Microtexture · Anisotropy · Hot-rolled steels

List of symbols

BTF	Brittle tilted fracture
RD	Rolling direction of the steel plate
TD	Transverse direction of the steel plate
ND	Normal direction of the steel plate
θ -Plane	Plane tilted by 40° around RD with respect to the rolling plane, along which BTF propagates
θ -Direction	Normal to the θ -plane
Anti- θ -plane	Plane tilted by 40° around TD with respect to the rolling plane
Anti- θ -direction	Normal to the anti- θ -plane
PCF	Potential cleavage facet, estimated from microtexture analyses
$PCF_{eff_s}^d$	Effective PCF size normal to the given loading direction d and relative to given steel S
$\alpha^{a,b}$	Misorientation angle between $\langle 001 \rangle$ directions of grain a and adjacent

F. Tankoua · J. Crépin · A.-F. Gourgues-Lorenzon (✉)
MINES ParisTech, MAT-Centre des Matériaux, PSL
Research University, UMR CNRS 7633, BP 87,
91003 Evry Cedex, France
e-mail: anne-francoise.gourgues@mines-paristech.fr

P. Thibaux · S. Cooreman
ArcelorMittal Global R&D Gent, Pres. J.F. Kennedylaan 3,
9060 Zelzate, Belgium

F. Tankoua
Present address: CEA Saclay, DEN/DANS/DM2S/SEMT/LISN,
91191 Gif-sur-Yvette, France

	grain b that are closest to the loading direction
α_c	Critical value of $\alpha^{a,b}$ used in the determination of PCFs
$\beta^{a,b}$	Misorientation angle between adjacent grains a and b
β_c	Critical value of $\beta^{a,b}$ used in the determination of PCFs
$\sigma_{c_s}^d$	Critical cleavage fracture stress estimated from notched tensile tests along loading direction d of steel S
$\sigma_{G_s}^d$	Critical cleavage fracture stress estimated from the Griffith-inspired approach along loading direction d of steel S
a	Exponent coefficient used for the calculation of $\underline{\sigma}_{eq}$
$\underline{\sigma}^{dev}$	Modified deviator of the stress tensor $\underline{\sigma}$
$\underline{\sigma}_{eq}$	Equivalent stress of the stress tensor $\underline{\sigma}$
ω^i	Minimum angle between the loading direction and a $\langle 001 \rangle$ direction of grain i
ω_c	Critical value of ω^i used in the determination of PCFs
c^i	Coefficients of the tensor used for the calculation of $\underline{\sigma}^{dev}$
R_0, H, Q, b	Hardening parameters of the Voce equation
σ_a, σ_b, T_0	Parameters of the R_0 versus temperature dependence equation

1 Introduction

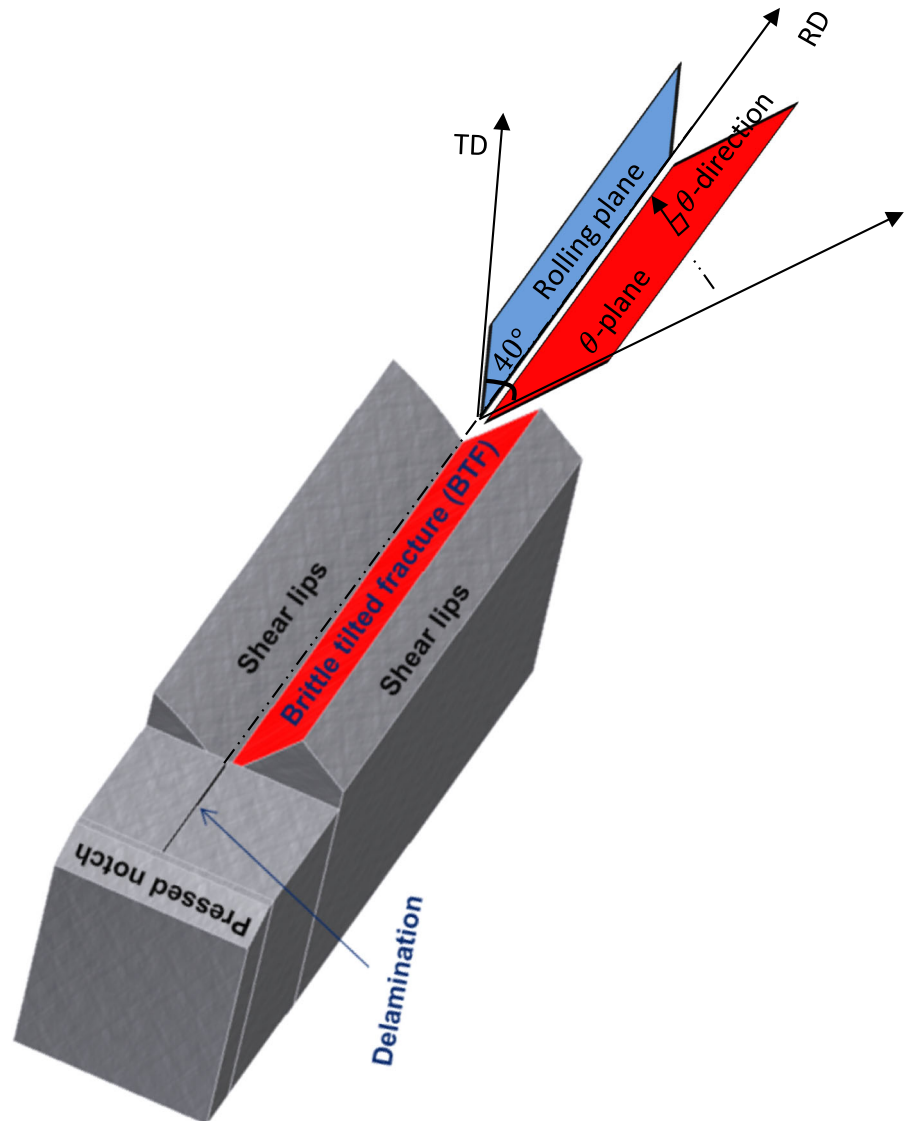
To take into account the global, increasing natural gas demand during the past decades, the gas pressure inside linepipes has been increased through the use of higher strength pipeline steels. Still, adequate toughness at low temperatures is required to avoid long brittle crack propagation. In the linepipe industry, the Battelle drop weight tear test (BDWTT) is commonly used as test method to assess the risk of long running brittle cracks as a reliable alternative to full-size burst tests like the West Jefferson test (Wilkowski et al. 1980; Cosham et al. 2009). In the BDWTT test, a three-point-bending notched specimen with the same thickness as the pipe

wall is impacted by a mass with a velocity of around 6.5 m/s. The ductile to brittle transition temperature is defined as the temperature at which the brittle area fraction, as measured by visual estimation after fracture reaches 15% of the total fracture area (ANSI/API 1996). BDWTT specimens have their long direction along the hoop direction such that the crack propagation direction is parallel to the axis of the pipe, as it is the direction of the maximum principal stress in service conditions. In case of so-called UOE-formed or High-Frequency Induction manufactured pipes, the hoop direction corresponds to the transverse direction of the skelp, while the pipe axial direction is parallel to the rolling direction.

Original research leading to the definition of the BDWTT in the 1970s established a good correlation between BDWTT and Charpy test results for the steel grades produced at that time by normalizing treatment. Unfortunately, this correlation is partly lost for steels obtained by more recent production techniques, such as thermo-mechanical controlled processing (TMCP). On the one hand, there is a difference in the assessment of impact toughness, namely, based on absorbed energy in the case of Charpy tests, and on fracture surface appearance for the BDWTT. Yet, this difference does not impede the correlation for normalized steels. On the other hand, in high strength TMCP steels, brittle cracks, non-perpendicular to the loading direction, have been reported within the ductile to brittle transition domain. Many of these brittle cracks occur by delamination along the rolling plane, especially in Charpy specimens (e.g. Baldi and Buzzichelli 1978; Bourell 1983; Mintz and Morrison 2007; Punch et al. 2012; Joo et al. 2012; Gervasyev et al. 2016b). However, especially in BDWTT specimens, the brittle crack may propagate along planes tilted by 40° around the main crack propagation direction (Hara et al. 2006, 2008; Fujishiro and Hara 2011) as schematically reported in Fig. 1. It is sometimes called “abnormal fracture” (Hwang et al. 2004; Yang et al. 2008), as well as “inverse fracture” (Hong et al. 2011; Sung et al. 2012). In the following, this phenomenon is more generally called “brittle tilted fracture” (BTF); the BTF plane (containing the rolling direction) will be referred to as the θ -plane, and the normal to that plane will be referred to as the θ -direction.

Brittle tilted fracture, which occurs within the ductile to brittle transition range, is clearly detrimental for the fracture resistance of pipeline steels, as it reduces the percentage of shear area and even the fracture

Fig. 1 Schematic view of a broken half of a BDWTT specimen, showing the orientation of θ -plane and θ -direction, as well as the occurrence of BTF after some propagation of a flat ductile crack. A delamination crack is also represented



energy (Hara et al. 2006) measured from BDWTT specimens. Only Hara et al. (2006) observed the occurrence of BTF in a Charpy specimen, yet with little detail. One plausible reason why BTF generally does not occur in Charpy specimens is that the ligament (8 mm, to be compared to 71 mm for BDWTT specimens), thus the crack propagation distance, is not long enough for BTF to occur. As a result, BTF is currently interpreted as a mechanical phenomenon related to the work hardenability of the steel (Hwang et al. 2004; Yang et al. 2008; Sung et al. 2012). The possible effects of microstructure-induced anisotropic cleavage fracture resistance (Hara et al. 2006, 2008) on the BTF phe-

nomenon have not been addressed yet. More generally, the anisotropy in critical cleavage fracture stress has mainly been assessed from Charpy tests using strong assumptions for mechanical analysis (plane strain loading, isotropic von Mises yield criterion) (Baldi and Buzzichelli 1978; Bourell 1983; Sun and Boyd 2000). Such assumptions might not apply to TMCP steels, as their strong anisotropic plastic flow requires more accurate analysis of mechanical tests. One of the aims of this work is to more accurately determine the anisotropy in critical cleavage fracture stress in this steel family.

The cleavage fracture resistance of steels has already been related to their microstructure. Cleavage cracks

may initiate from non-metallic inclusions (e.g. [Rosenfield et al. 1983](#); [McRobie and Knott 1985](#)), coarse carbides ([Bowen et al. 1986](#); [McRobie and Knott 1985](#)) or martensite-austenite constituents ([Lambert-Perlade et al. 2004](#); [Di Shino and Guarnaschelli 2010](#)). They propagate along {001} planes of the bcc crystal structure of ferrite (or bainitic ferrite) (see e.g. [Gervasyev et al. 2016b](#) for the case of an X80 pipeline steel) until a high angle grain boundary is encountered ([Bouyne et al. 1998](#); [Gourgues et al. 2000](#)). The distance between such boundaries is considered the unit cleavage crack path. In bainitic steels, it relates to their particular microtexture inherited from decomposition of austenite ([Brozzo et al. 1977](#); [Bouyne et al. 1998](#); [Gourgues et al. 2000](#)).

In hot-rolled ferritic steels, the relationship between the ferrite grains and the unit cleavage crack path is less clear. The average texture anisotropy has been used to derive microstructural criteria based on fractions of grains that exhibit a {001} plane perpendicular to a given loading direction, within a certain tolerance angle ([Bourell 1983](#); [Kotrechko et al. 2004](#); [León García et al. 2007](#); [Sanchez Mouriño et al. 2010](#); [Joo et al. 2012](#); [Zong et al. 2013](#)). For instance, the strong effect of the {001}⟨110⟩ rotated cube component on the sensitivity to brittle delamination has been underlined for a long time (e.g. [Bourell 1983](#); [Zong et al. 2013](#); [Gervasyev et al. 2013, 2016b](#)), but not on a grain-by-grain basis. The so-called ‘cleavage morphology clustering’ approach ([Gervasyev et al. 2013, 2016a](#)) combined average information obtained from electron backscatter diffraction (EBSD) on grain size and morphology (determined irrespectively of their crystal orientation) together with the intensity of the rotated cube texture component (determined irrespectively of the size and morphology of individual grains). In TMCP steels, the competition between brittle delamination and BTF could be related to the relative intensity and spatial distribution of {100} crystal planes parallel to the rolling plane and to θ -planes, respectively ([Baldi and Buzzichelli 1978](#); [Hara et al. 2006, 2008](#)). However, no correlation has been reported yet with the actual morphology and size of cleavage facets of the fracture surfaces. In order to relate the resistance of ferritic steels to cleavage cracking to their microstructure and local texture at the grain scale, the local concept of ‘potential cleavage facets’ (PCFs), i.e., clusters of grains sharing {001} planes closely oriented to each other and perpendicular to a given loading direction, has been briefly presented ([Tankoua et al. 2014a, b](#)) and

is assessed in more detail in this work. Another recently reported determination of these regions, the so-called ‘cube grain clusters’ ([Ghosh et al. 2016a, b](#)) will also be discussed.

The present work aims at determining the respective contributions of plastic flow anisotropy and microstructural anisotropy to the BTF and delamination phenomena in BDWTT, and, more generally, at setting up a methodology to quantitatively link the cleavage fracture resistance of ferritic steels to their microtexture (instead of their gross texture). According to the local approach to brittle fracture, mechanical analysis of the experimental tests was carried out to estimate the local stress state at the experimentally observed fracture initiation sites. To this aim, static tests on notched tensile bars were chosen in order to avoid contact and dynamic loading issues in the numerical analysis, which are encountered in bending impact tests. A critical cleavage fracture stress was estimated for various loading directions: in-plane RD and TD directions commonly used in impact and tensile tests, as well as the normal to the plate (ND) (sensitivity to delamination by brittle cleavage cracking) and the θ -direction (sensitivity to BTF). To determine the stress at the crack initiation site, the mechanical tests were analysed by means of finite element calculations, taking into account the anisotropic constitutive behaviour. On the other hand, the anisotropy in microtexture along the corresponding planes was also quantified using the PCF concept and compared to that in cleavage cracking resistance.

2 Materials and experimental procedures

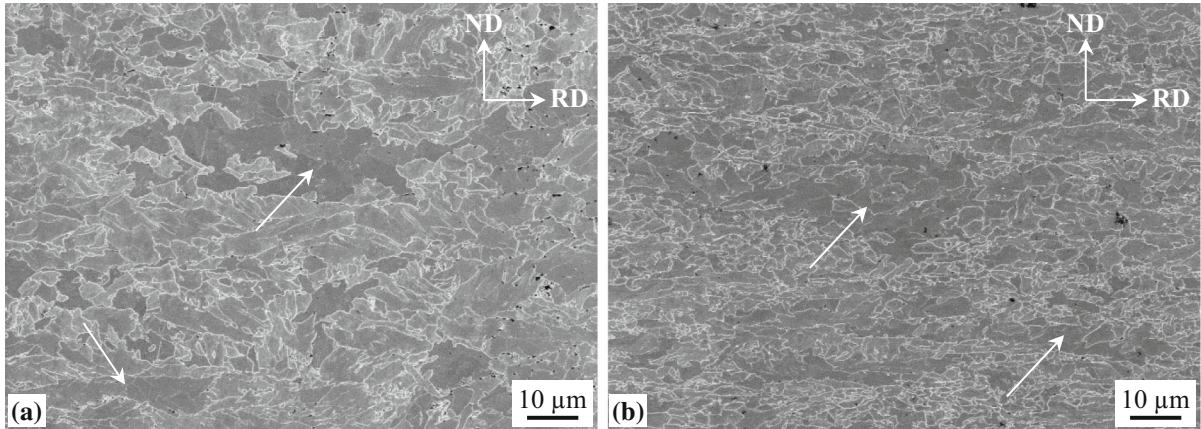
2.1 Materials

Two hot-rolled, ferritic-bainitic API 5L grade X70 steels were selected for the study. Their thickness was 19.5 mm for Steel A and 23 mm for Steel B. The microtexture and cleavage sensitivity of Steel A have already been reported elsewhere ([Tankoua et al. 2014a, b](#)), yet without a quantitative link between them. In the present work, these results are further analysed together with new results obtained for Steel B.

The chemical composition of both steels is reported in Table 1. Their typical microstructure (Fig. 2) was composed of fine ferritic grains of 1–5 μm in size. Larger entities (some of them being arrowed in Fig. 2), resembling larger grains with internal subboundaries

Table 1 Chemical composition (wt%) of Steels A and B

	C	Mn	Si	P	Ni + Cr + Mo	Al	Ti + Nb	Cu	S
Steel A	0.047	1.2	0.24	0.013	0.64	0.02	0.083	0.31	0.0025
Steel B	0.031	1.7	0.21	0.013	0.40	0.05	0.138	0.28	0.0018

**Fig. 2** Scanning electron micrographs of **a** Steel A and **b** Steel B (secondary electron images, nital etching). Some elongated large entities are indicated with white arrows

and irregular in shape, were also found. They were up to 30 μm in size for Steel A and somewhat finer for Steel B. They appeared slightly elongated along RD. Except for these larger entities, no significant anisotropy in grain size or aspect ratio was evidenced from micrographs taken from the (RD, TD), (RD, ND) and (TD, ND) planes, respectively.

The non-metallic inclusions of the two steels were mainly small, equiaxed aluminium- and magnesium-rich oxides, sometimes combined with calcium-containing sulphides, with an average size lower than 2 μm and an area fraction of about 0.025%. None of these inclusions was ever found at any cleavage initiation site in the present work, so they were not considered to play a major role in the fracture process. Unlike in higher carbon steels (e.g. Ghosh et al. 2016a, b), neither a hard secondary phase nor clusters of coarse carbides, that could have dominated cleavage crack initiation, were found. In contrast with other low-carbon pipeline steels of higher strength (e.g. Joo et al. 2012), no pronounced microstructural banding was observed.

The Vickers hardness (300 g load, 10 s dwell time) was 210 ± 10 and 220 ± 10 for Steels A and B, respectively, with no significant gradient across the plate thickness. Their average texture, determined using X-

ray diffraction at mid-thickness along the (RD, TD) plane, was typical of high strength, hot-rolled steels, with a slight $\{001\}\langle 1\bar{1}0\rangle$ rotated cube component and a partial $\{111\}\gamma$ -fibre, with an intensity less than, respectively, 5 times and 3 times that of a random texture in a $\varphi_2 = 45^\circ$ view of the orientation distribution function.

2.2 Impact testing

Battelle drop weight tear tests were performed on pressed notch specimens taken along TD with the crack propagating along RD (TD–RD geometry), according to API 5L3 standard (ANSI/API 1996). Full thickness specimens were used for Steel A (19.5 mm). For Steel B, the plate thickness was reduced from both sides from 23 to 19 mm, as described in API 5L. These tests were done on instrumented BDWTT equipment, with a hammer of 985 kg and a drop height of 2.19 m. The maximal energy provided by the hammer was 21 kJ and the hammer speed at the impact was 6.5 m s^{-1} . Specimens were cooled down to various temperatures between 0 and -100°C by immersion into a specific liquid mixture for temperatures above -70°C and in a climate chamber for temperatures below -70°C . The anisotropy in

impact behaviour, and in particular, in the sensitivity to BTF, was addressed by testing a few specimens of Steel B taken along RD with the crack propagating along TD (RD–TD geometry) after slight flattening by four-point bending because of the curvature of the hot-rolled coil. The load versus displacement curve, impact energy and shear area ratio were determined for each test to assess the ductile-to-brittle transition behaviour of both steels.

2.3 Tensile testing

The sensitivity to cleavage cracking was investigated by using tests on round notched tensile bars, referred to as NT specimens hereafter. The specimen geometry was optimised by finite element calculations (Tankoua 2015) to ensure that (1) they could be cut along any direction of the coil, including ND and the θ -direction, (2) the plastic zone developed from the notched region would never reach the specimen ends, and (3) a significant stress triaxiality could be achieved in order to trigger cleavage cracking in a region containing at least several of the larger entities determined by microstructural analysis (Fig. 2). In this way it was not required to weld elongation pieces to notched specimens to examine the sensitivity to cleavage cracking perpendicular to ND (i.e., in the delamination plane) as done in Baldi and Buzzichelli (1978) and Gervasyev et al. (2016b). A maximal diameter of 5 mm, a minimal diameter of 2.6 mm and a U-notch radius of 0.4 mm were used, except for Steel A specimens cut along RD and TD, for which a notch radius of 0.6 mm was used.

The tensile tests on NT specimens were performed on a 250 kN servohydraulic Instron 8500 machine. The notch geometry of every specimen was measured by using a shape projector (accuracy of 10 μm). Before starting every test, the minimal diameter of the specimen was measured and the knives of the radial extensometer were fixed to measure the diameter reduction along ND at the minimal section for tests along RD and TD. For tests along ND, the diameter reduction was measured along TD; for tests along the θ -direction the diameter reduction was measured along RD. The location of the knives was validated after comparing the diameter measured by the extensometer and the one obtained from the shape projector equipment. At least two specimens were tested per condition. The effective stress was calculated as the load divided by the initial value of the minimal section and the diameter reduction

was normalized by the initial diameter of the minimal section.

Isothermal tensile tests were performed with a prescribed load line displacement rate of $5 \times 10^{-3} \text{ mm s}^{-1}$. The test temperature was set to $-196 \text{ }^\circ\text{C}$ by immersion in liquid nitrogen. As specimens of Steel A tested along ND exhibited an unusual fracture mode that was out of the scope of the present study, similar tests were also performed along that direction at $-100 \text{ }^\circ\text{C}$ (for which only flat cleavage fracture occurred) by using a climate chamber. The fracture surfaces were observed by scanning electron microscopy (SEM) to investigate the fracture mode and to locate cleavage initiation sites.

The plastic flow behaviour of Steels A and B was also determined from uniaxial tensile (UT) tests on smooth specimens. For the tests along RD and TD, specimens with a gauge diameter of 4 mm and a gauge length of 36 mm were used, while specimens with a gauge diameter of 2.6 mm and a gauge length of 5 mm were used for the tests along ND and θ -direction. A longitudinal extensometer of respectively 10 and 5 mm in gauge length was used to monitor elongation. The test temperature was set up as for the NT specimens. An elongation rate of 10^{-3} s^{-1} was prescribed. The anisotropy in plastic behaviour was extracted from (1) the stress-strain curves and (2) the Lankford coefficients, which were determined from post mortem measurements on the fracture surfaces. Such measurements assume that cleavage fracture itself did not significantly modify the geometry of that particular plane of the specimen, which appears to be reasonable in the present case of fully flat cleavage fracture. More precisely, the Lankford coefficients were defined as the ratio of the lower reduction in diameter to the higher one. As the shape of the fracture surfaces appeared elliptic, the considered directions were perpendicular to each other. The spatial orientation of the considered diameters was recorded with respect to the (RD, TD, ND) frame to allow comparison between experimental results and prediction from the numerical model (see Sect. 3.2.1).

2.4 Microstructural quantification of the sensitivity to cleavage cracking

Particular attention was paid to the spatial and size distribution of grains that exhibited a $\{100\}$ plane almost perpendicular to a given loading axis, more specifically,

to the anisotropy in size distribution and total fraction of PCFs. They were quantitatively studied by EBSD mapping along planes, respectively, perpendicular to the ND, θ , RD, and TD directions. As BDWTTs were also carried out on RD–TD specimens, the possibility of BTF for that specimen orientation, with the same geometry as for the conventional TD–RD specimens, was also considered. The corresponding plane, tilted by 40° around TD with respect to the (RD, TD) plane, as well as its normal are denoted, respectively, as the anti- θ -plane and the anti- θ -direction hereafter.

In order to accurately characterise fine ferrite grains while limiting sampling effects due to long-range spatial variations in microtexture, EBSD analysis was carried out over a large field ($1\text{ mm} \times 0.5\text{ mm}$) resulting from the merging of eight neighbouring maps ($250\text{ }\mu\text{m} \times 250\text{ }\mu\text{m}$), to obtain statistically relevant results, covering at least one hundred of larger entities. A fine step size ($0.5\text{ }\mu\text{m}$, i.e. 10 times lower than the average grain size) was used to catch every detail of the matrix microstructure. This analysis was done in a field emission gun (FEG) scanning electron microscope (under magnification $\times 350$) using the following EBSD setup parameters: high voltage 30 kV, tilt angle 70° , working distance 17 mm. More than 99.8% of points were reliably indexed. A grain dilation clean-up procedure was applied with a grain tolerance angle of 5° and a minimum grain size of 5 pixels.

To determine the maximum deviation angle allowing continuous propagation of cleavage microcracks, quantitative fractography was performed on a NT specimen exhibiting large cleavage facets at the crack initiation site. First, images of the first cleavage facets were taken with SEM at high magnification, at tilt angles of -6° , 0° , and $+6^\circ$. From these three images, a 3D reconstruction of the zone of interest was obtained (by the so-called “stereological pairs” method) using the MeX software. Then, local misorientations of the fracture surface were determined both within the first cleavage facet (continuous crack propagation shown by some continuity in cleavage rivers) and between that facet and its neighbours (i.e. involving arrest of that first cleavage microcrack). The tilt and twist components were calculated from the actual local orientation of the fracture surfaces, by assuming a fictitious boundary parallel to the specimen axis. Thus, the particular values of tilt and twist angles should be considered approximate.

3 Results

3.1 Impact toughness behaviour

Figure 3 shows the ductile-to-brittle transition behaviour for both steels, described both in terms of the shear area percentage and fracture energy. When considering the 50% shear area percentage obtained for the usual (TD–RD) specimens, the transition temperature was -60°C for both steels. No obvious difference in fracture energy or shear area percentage was noticed between the two steels. On the other hand, despite the limited number of tested specimens, Steel B showed a slightly lower shear area percentage transition temperature (-70°C) for (RD–TD) specimens than for (TD–RD) specimens.

The different shapes of load versus displacement curves are schematically represented in Fig. 4a. Careful examination of all fracture surfaces allowed relating the various parts of these curves to the crack propagation modes observed in the fractured specimens.

By increasing the test temperature, the following fracture modes were observed at the macroscopic scale in TD–RD oriented specimens (Fig. 4a):

- (1) Brittle fracture initiated from the notch root, then propagated along the entire ligament, without shear lips. This was only the case for two specimens of Steel A ($T = -100^\circ\text{C}$).
- (2) Brittle fracture initiated from the notch root, then propagated along the entire ligament, together with shear lips ($-100^\circ\text{C} < T < -60^\circ\text{C}$).
- (3) Brittle fracture initiated from the notch root turned into BTF. BTF is followed by ductile slant fracture ($-60^\circ\text{C} < T < 0^\circ\text{C}$).
- (4) Brittle fracture initiated from the notch root, then turned into ductile slant fracture along the rest of the ligament ($-60^\circ\text{C} < T < 0^\circ\text{C}$).
- (5) Ductile slant fracture initiated from the notch root after some flat ductile crack propagation. It was followed by BTF which propagated along the entire ligament ($-60^\circ\text{C} < T < 0^\circ\text{C}$).
- (6) Ductile slant fracture initiated from the notch root after triangular ductile crack propagation. It was followed by BTF which turned into a final ductile slant fracture ($-60^\circ\text{C} < T < 0^\circ\text{C}$).
- (7) Full ductile slant fracture occurred ($T > 0^\circ\text{C}$).

According to the API 5L3 standard (ANSI/API 1996), a BDWTT test is only valid if the broken specimen exhibits brittle crack initiation at the notch root,

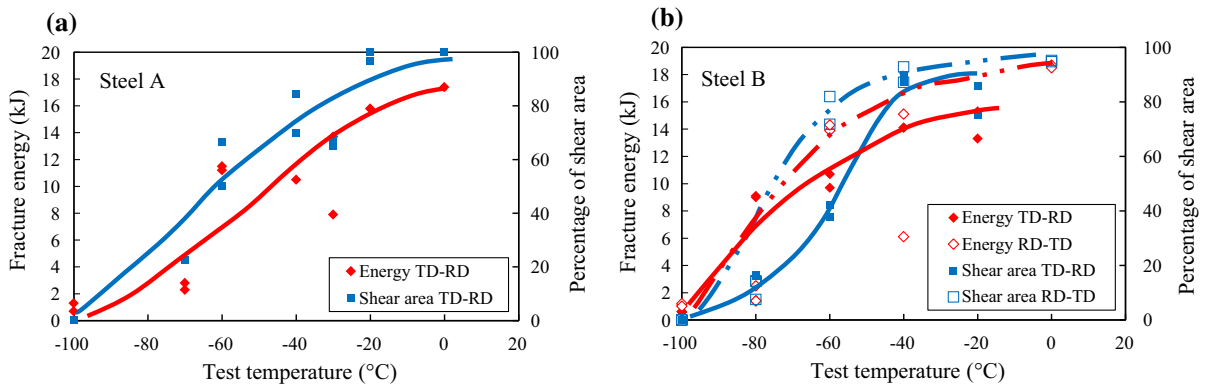
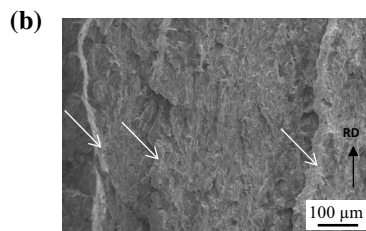
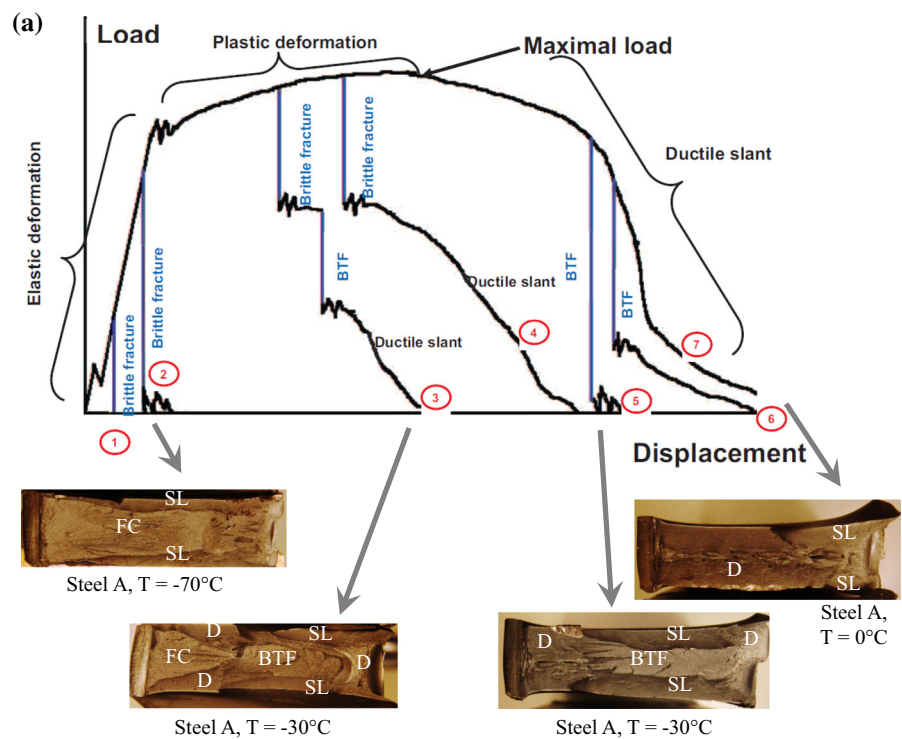


Fig. 3 Ductile-to-brittle transition curves of **a** Steel A and **b** Steel B in both shear area and fracture energy. Solid (resp. broken) lines have been added to facilitate visualisation for TD–RD (resp. RD–TD) orientations

Fig. 4 a Schematic load versus displacement curves from instrumented BDWTTs, associated to typical fracture modes (optical macrographs). TD–RD specimens, the notch is on the left. *D* ductile, *SL* shear lips, *FC* flat cleavage, *BTF* brittle tilted fracture. **b** Detailed view of BTF in a TD–RD specimen of Steel B tested at -30°C : cleavage fracture along macroscopically tilted planes, linked by ductile slant fracture ligaments (white arrows)



which turns into ductile slant fracture, unless the entire fracture surface is either brittle or ductile. This was not the case in the present work, because ductile crack initiation or BTF occurred in many cases. Indeed, with the high ductility of modern pipeline steels, brittle fracture initiation at the notch is more difficult. The use of a machined notch (chevron) or of a pre-cracked notch has been proposed in literature (Hwang et al. 2004) but was not adopted here as it is not accepted in all standards (EN 2013).

Brittle tilted fracture was observed for temperatures lower than -30°C for Steel A and -20°C for Steel B (TD–RD) specimens, respectively. Within the propagation region of BTF, entities similar to macroscopic rivers were observed (see e.g. Fig. 4, case 5). These macroscopic rivers were more pronounced far from the initiation site. SEM observations of the fracture surface were performed after tilting the specimen by 40° around RD, so that the BTF surface became perpendicular to the incident electron beam. A stair-shaped fracture mode was observed around macroscopic rivers, i.e., cleavage fractured θ -planes were linked to each other by ductile slant regions (Fig. 4b). This suggests that BTF propagates along more than one θ -plane at a time.

Brittle tilted fracture, as well as flat cleavage fracture led to a drop in load (cases 3–6 in Fig. 4a). The larger the area of BTF on the fracture surface, the more pronounced the drop in load. Consequently, BTF reduced the impact fracture energy. The occurrence of delamination was not associated to any abrupt drop in load. Nevertheless, it might accelerate the decrease in load during ductile crack propagation, since it introduces damage within the specimen. In Steel A (but rarely in Steel B), a brittle delamination crack was observed in

some instances to rotate toward the plane perpendicular to the main loading direction. The occurrence of this so-called delamination rotation was not obviously noticeable on the load versus displacement curves, perhaps because it happened rather close to the back of the specimen. Delamination rotation brings additional brittle fracture area that is taken into account for the shear area calculation. As such, the sensitivity to (brittle) delamination cracking should not be ruled out from the assessment of impact toughness of this steel family.

In RD–TD oriented specimens, within the ductile-to-brittle transition region, brittle out-of-plane cracking was identified as delamination, which rotated to join either the main loading plane, or the θ -plane (which was here parallel to the loading direction). No BTF, i.e., no brittle cracking along the anti- θ planes, was observed for this specimen orientation.

3.2 Tensile behaviour

3.2.1 Uniaxial tensile behaviour

The anisotropy in strength was very weak for both steels under uniaxial tension (Fig. 5), although the steels exhibited a yield point when tested along certain directions only. A low level of work hardening was noticed whatever the loading direction. On the other hand, a Lankford coefficient from 0.7 ± 0.05 to 0.85 ± 0.05 was determined from fracture surfaces of specimens tested at -196°C , for which necking was not pronounced. As a result, anisotropic plastic flow had to be taken into account in the constitutive model of Steels A and B for accurate determination of cleavage fracture initiation conditions.

Fig. 5 Uniaxial tensile curves at -196°C : experimental results and model predictions for **a** Steel A and **b** Steel B

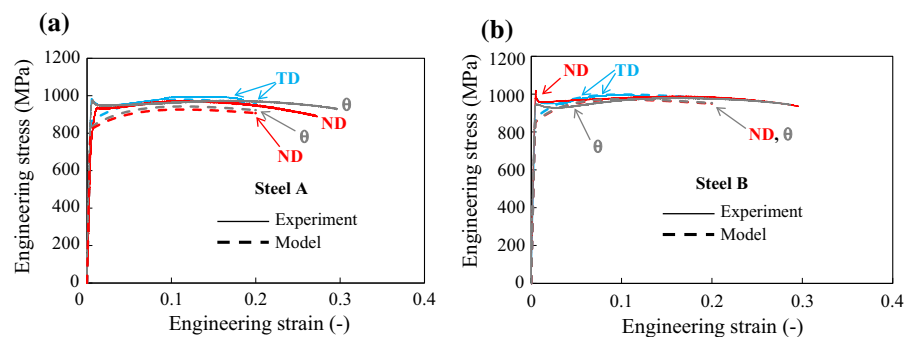
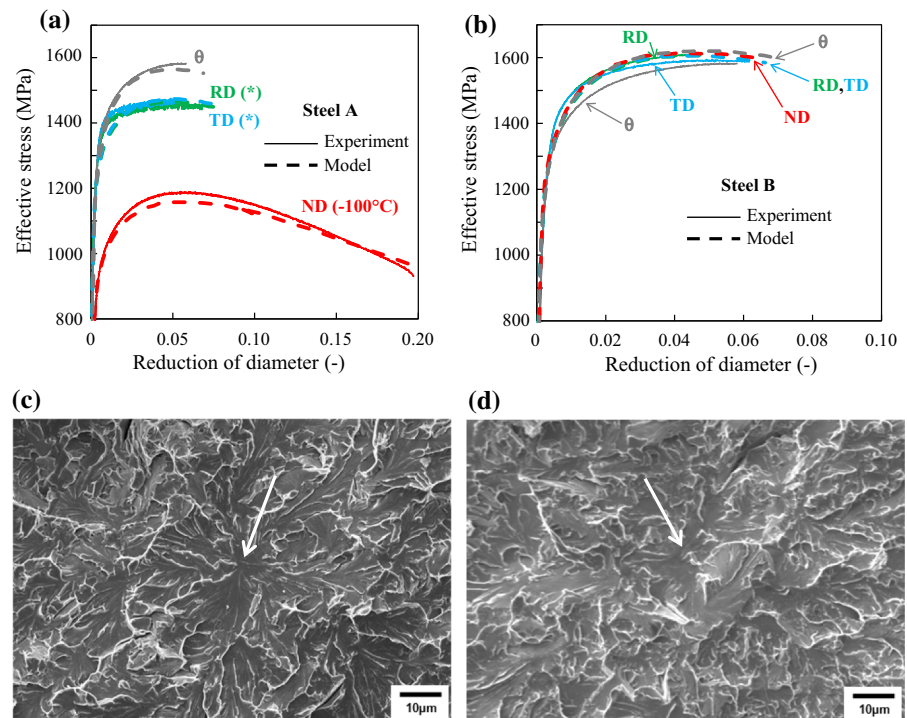


Fig. 6 Effective stress versus diameter reduction curves of NT specimens tested at -196°C (unless otherwise stated) for **a** Steel A and **b** Steel B. (*) modified NT geometry (notch radius 0.6 mm instead of 0.4 mm). **c, d** Fracture initiation site of NT specimens of **c** Steel A tested along ND at -100°C and **d** Steel B tested along ND at -196°C



3.2.2 Tensile behaviour of notched specimens

The effective stress versus diameter reduction curves (Fig. 6) showed very low reduction in diameter at fracture (except for Steel A tested along ND at -100°C). In all specimens, brittle, flat cleavage fracture was found and the location of the cleavage initiation site, determined by SEM, was far from the notch root. Along ND, fracture initiated from a 60- μm -large facet in Steel A (Fig. 6c), and from a 25- μm -large facet in Steel B (Fig. 6d). Unlike, for example, in Gervasyev et al. (2016b), no particle was found at the cleavage initiation site on unetched fracture surfaces. This was confirmed by examination of specimens tested at various temperatures in another part of this research work (Tankoua 2015). In specimens loaded along TD, cleavage initiated close to a delamination microcrack for the two steels. In specimens loaded along RD, along ND and along the θ -direction, neither delamination nor inclusion were found at the fracture initiation site, although delamination microcracks were found elsewhere in Steel A specimens tested along RD (but not in those tested along TD).

3.3 Determination of critical cleavage fracture stresses

3.3.1 Modelling the tensile tests on NT specimens

Constitutive equations used to represent the plastic flow behaviour of Steels A and B had to account for the low stress anisotropy and for the significant strain anisotropy evidenced by Lankford coefficients far from 1. Although it is the most popular anisotropic model, the yield criterion proposed by Hill (1950) is not suited to this case. Therefore, the one proposed by Barlat et al. (1991) was selected. In this model, with $\underline{\sigma}$ the stress tensor and p the equivalent plastic strain, the yield surface is defined as:

$$f(\underline{\sigma}, p) = \underline{\sigma}_{eq} - R(p) \quad (1)$$

The equivalent stress, $\underline{\sigma}_{eq}$, is expressed as follows:

$$\underline{\sigma}_{eq} = \frac{1}{2} \left(|\sigma_1^{dev} - \sigma_2^{dev}|^a + |\sigma_2^{dev} - \sigma_3^{dev}|^a + |\sigma_3^{dev} - \sigma_1^{dev}|^a \right)^{1/a} \quad (2)$$

In this equation, $\sigma_1^{dev} \geq \sigma_2^{dev} \geq \sigma_3^{dev}$ are the eigenvalues (i.e., principal values) of the modified stress deviator, $\underline{\sigma}^{dev}$, obtained as a linear function of the stress tensor, as follows:

$$\underline{\underline{\sigma}}^{dev} = \underline{\underline{S}} : \underline{\underline{\sigma}}, \quad \text{with}$$

$$\underline{\underline{S}} = \begin{pmatrix} \frac{c_2+c_3}{3} & -\frac{c_3}{3} & -\frac{c_2}{3} & 0 & 0 & 0 \\ -\frac{c_3}{3} & \frac{c_1+c_3}{3} & -\frac{c_1}{3} & 0 & 0 & 0 \\ -\frac{c_2}{3} & -\frac{c_1}{3} & \frac{c_1+c_2}{3} & 0 & 0 & 0 \\ 0 & 0 & 0 & c_4 & 0 & 0 \\ 0 & 0 & 0 & 0 & c_5 & 0 \\ 0 & 0 & 0 & 0 & 0 & c_6 \end{pmatrix}$$

(in Voigt notations) (3)

The isotropic hardening, $R(p)$, was described using a yield stress, R_0 , a linear contribution (involving parameter H) and an exponential Voce-type term (involving parameters Q and b):

$$R(p) = R_0 + Hp + Q(1 - \exp(-bp)) \quad (4)$$

In this model, the eleven constitutive parameters to be identified are: R_0 , H , b , Q , a , and c_{1-6} . Uniaxial tensile tests were modelled using a single volume element. Tests on NT specimens were modelled by using the finite element method and the Z-set in-house software (Besson and Foerch 1997). From a parametric numerical study reported elsewhere (Tankoua 2015), three-dimensional meshes made of quadratic, eight-node elements with reduced integration were used. One-eighth of the specimen was modelled, together with the usual symmetry conditions and a prescribed uniform axial displacement at the specimen end, along the loading axis. A mesh size of 400 μm was found fine enough for the load versus displacement (or diameter reduction) curves predicted by the model to be independent of meshing. It was thus used in the iterative procedure to optimise the set of constitutive model parameters. For the determination of the critical cleavage fracture stresses, following another mesh convergence study (Tankoua 2015), a single calculation using a finer mesh (15 μm in size close to the specimen centre) was carried out. A Newton–Raphson global scheme was used, together with an implicit integration method and finite strain formalism for the constitutive behaviour, based on the use of a local objective frame as proposed in Besson et al. (2009). Observer invariant stress and strain rate measures were defined by transport of the Cauchy stress and strain rate into the corotational frame characterised by a rotation Q (function of both space coordinates and time). An experimental database larger than that reported here (Tankoua et al. 2014a; Tankoua 2015), including tests at various temperatures between -196°C and room temperature, was used to identify model parameters from

tests on smooth and NT specimens, including information on strain anisotropy. The dependence of R_0 on the test temperature followed an exponential function of absolute temperature, $R_0 = \sigma_a + \sigma_b \exp(-T/T_0)$, T being the test temperature (in Kelvin) and σ_a , σ_b , T_0 being material parameters, with an accuracy better than 10 MPa (Tankoua 2015). The values of σ_a , σ_b , and T_0 for Steel A (resp. Steel B) were 478 MPa (540 MPa), 1036 MPa (1020 MPa) and 76.9K (71.4 K), respectively. The strain hardening behaviour was found to be independent of temperature for temperatures up to -100°C , so that hardening parameters were adjusted at -100°C (Tankoua 2015). Parameters describing flow anisotropy were adjusted at room temperature, for which a larger database was available, and validated using the ratio between minimal and maximal reductions in diameter as measured on smooth specimens fractured at -196°C . More details can be found in (Tankoua 2015). No remarkable variation in the notch radius was observed between the various specimens, but there was a little variation in the minimal diameter value between 2.55 and 2.63 mm depending on the specimen, so that the actual geometry of every notch was modelled in the numerical simulation on an individual basis.

The optimised sets of parameters identified for both steels are reported in Table 2. As both steels showed similar plastic flow properties, the values of their constitutive parameters are close to each other. Figures 5 and 6, as well as Table 3 show good agreement between experimental values and model predictions, with an average difference of 5% in strength and a fairly good estimate of Lankford coefficients, even if the strain anisotropy was underestimated by the best set of model parameters. These results allowed estimation of the critical cleavage fracture stresses from the finite element analysis of the tests on NT specimens.

3.3.2 Derivation of critical cleavage fracture stresses

For any loading direction, d , and for any of the two steels, S ($S = \text{Steel A or Steel B}$), the critical cleavage fracture stress along that direction, σ_{c-S}^d , was estimated from the corresponding tests on NT specimens loaded along direction d . Two tests per direction were used. Numerical calculations were stopped at the diameter reduction measured at the onset of brittle fracture; σ_{c-S}^d was then determined as the axial stress at the location of the experimentally observed cleavage initiation site.

Table 2 Constitutive model parameters identified for Steel A and Steel B at liquid nitrogen temperature. For Steel A at -100°C , $R_0 = 587\text{ MPa}$

	R_0 (MPa)	H (MPa)	Q (MPa)	b	a	c_1	c_2	c_3	c_4	c_5	c_6
Steel A	859	430	220	17	12	1.038	1.057	0.952	1.041	1.034	1.032
Steel B	887	682	180	26	12	1.028	1.034	0.982	0.999	1.032	1.062

Table 3 Comparison between experimentally measured and predicted Lankford coefficients (measured using the same directions) for both steels and various orientations of the uniaxial tensile stress

Steel/loading direction + definition of Lankford ratio	RD $\varepsilon_{TD}/\varepsilon_{ND}$	TD $\varepsilon_{RD}/\varepsilon_{ND}$	ND $\varepsilon_{TD}/\varepsilon_{RD}$	θ -direction $\varepsilon_{RD}/\varepsilon_{perpendicular}$
A				
Experiment	(Not available)	0.73	0.80	0.77
Model		0.70	1.01	0.87
B				
Experiment	0.71	0.83	0.86	0.80
Model	0.81	0.83	1.02	0.89

An uncertainty of $\pm 50\text{ MPa}$ on σ_{c-s}^d was estimated for this determination, owing to both the uncertainty related to the constitutive model and the maximal variation in axial stress over a distance of $100\ \mu\text{m}$ around the crack initiation site. Since this value of $100\ \mu\text{m}$ was larger than twice the average size of both ferrite grains (see Fig. 2) and of PCFs (as will be shown below), the characteristic distance of at least two times the grain size, requested by the so-called Ritchie–Knott–Rice local approach to fracture (Ritchie et al. 1973), was fulfilled. In some cases, because of the presence of delamination cracks that act as stress concentrators, the actual local cleavage fracture stresses are supposed to be higher than those determined by applying the present delamination-free modelling approach to these particular specimens. As a consequence, only a lower bound of σ_{c-A}^{RD} , σ_{c-A}^{TD} , and σ_{c-B}^{TD} could be determined, by considering the higher axial stress within the specimen (at the centre), but not considering the mechanical influence of the (already present) delamination crack. In the absence of delamination, the two tests per condition yielded critical cleavage fracture stress values close to each other. The values of σ_{c-s}^d are reported in Table 4.

Except for Steel A tested along ND (i.e. fractured along the (RD, TD) plane), all values of σ_{c-s}^d are higher than 2000 MPa , showing good resistance to cleavage cracking. By comparing the values of σ_{c-B}^{ND} and σ_{c-B}^θ , Steel B appears more sensitive to cleavage cracking

along the θ -plane than along the rolling plane. Steel A seems very sensitive to cleavage along the rolling plane but the value of σ_{c-A}^{ND} was determined from a material elongated (in average) by at least 30% (corresponding to a diameter reduction of 0.15), whereas all other NT specimens fractured with a diameter reduction lower than 0.07. In both steels, the cleavage fracture resistance for $d = \text{RD}$ and $d = \text{TD}$ was higher than that for $d = \text{ND}$ and $d = \theta$ -direction. This could explain why in BDWTT specimens tested along TD, BTF strongly competes with flat cleavage fracture in the ductile-to-brittle transition temperature range.

3.4 Microtexture quantification

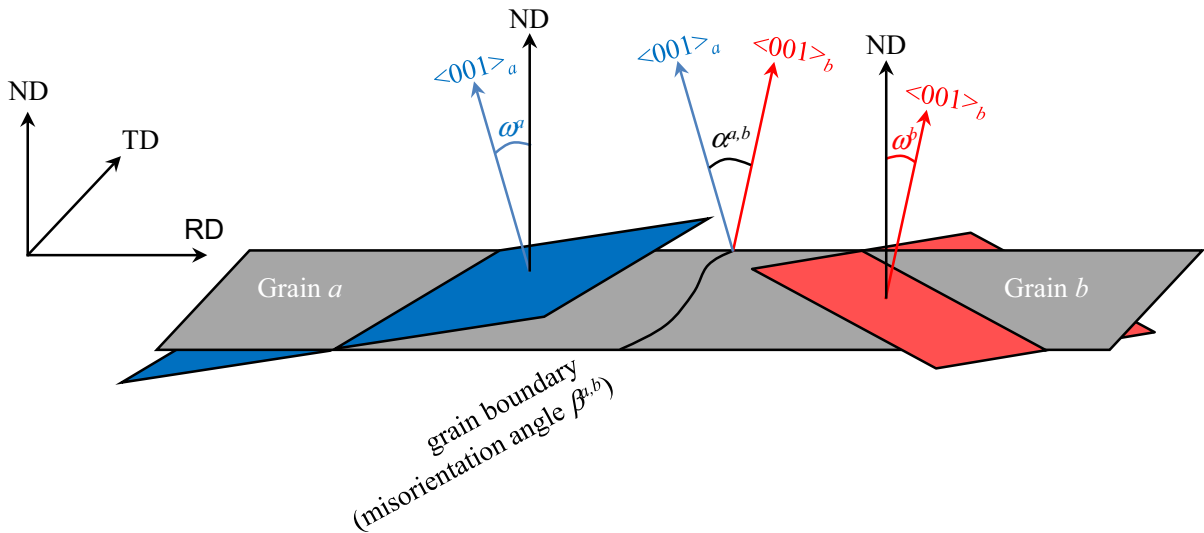
3.4.1 Setting up the microtexture quantification method

To link the anisotropy in sensitivity to cleavage cracking with the steel microtexture, EBSD maps were used to quantify the PCF area fraction and size distribution. To set up the quantification method, the (RD, TD) plane of Steel A was chosen because of its rather heterogeneous microstructure containing large entities resembling clusters of slightly misoriented grains (Fig. 2) together with rather large facets at the origin of cleavage fracture along that plane. A $1\text{ mm} \times 0.5\text{ mm}$ EBSD

Table 4 Quantification of microtexture (PCF area fraction, effective PCF size) and estimates of the critical cleavage fracture stress ($\sigma_{c_s}^d$ from FE analysis and $\sigma_{G_s}^d$ from the Griffith-inspired approach of Eq. 5) along different planes of Steels A and B

Plane perpendicular to loading direction d	(RD, TD)	θ	Anti- θ	(TD, ND)	(RD, ND)
Steel A					
PCF area fraction	26.7%	12.7%	5.8%	5.2%	7.8%
Effective PCF size, $PCF_{eff_A}^d$ (μm)	18.1	12.3	10.6	10.2	11.1
Critical cleavage fracture stress from FE analysis, $\sigma_{c_A}^d$ (MPa)	1800 (*)	2200	(No test)	> 2200	> 2200
Critical cleavage fracture stress from Griffith-inspired model, $\sigma_{G_A}^d$ (MPa)	1440	2130	(No test)	2510	2330
Steel B					
PCF area fraction	13.4%	20.2%	6.0%	8.9%	5.9%
Effective PCF size, $PCF_{eff_B}^d$ (μm)	11.6	12.7	9.7	10.7	10.3
Critical cleavage fracture stress from FE analysis, $\sigma_{c_B}^d$ (MPa)	2200	2000	(No test)	2400	2500
Critical cleavage fracture stress from Griffith-inspired model, $\sigma_{G_B}^d$ (MPa)	2240	2000	(No test)	2410	2500

(*) test at -100°C with significant reduction of area at fracture (around 0.15)

**Fig. 7** Definition of deviation angles for the quantification of PCFs

map was used to calibrate the microstructural quantification method.

As illustrated in Fig. 7, only the grains having a $\{001\}$ plane normal, i.e. a $\langle 001 \rangle$ direction, “sufficiently” close to the loading direction (i.e., misoriented by an angle, ω^i , lower than a critical angle, ω_c) were considered to possibly belong to (hereafter, to be “eligible to”) a PCF. In fracture surfaces, the first cleavage facet was sometimes clearly not perpendicular to the loading direction, so that the value of ω_c had to be set rather far from 0° . This could stem from the fact that at the grain scale, the direction of the local maximum prin-

cipal stress is not necessarily close to the macroscopic tensile axis. The following values of ω_c were tested: 5° , 10° , 15° , 20° , and 25° , respectively. As expected, the area fraction covered by PCFs increases with ω_c (see inset in Fig. 8). Moreover, from the curves in Fig. 8, increasing the value of ω_c increased the area fraction of larger PCFs and, more generally, of all PCFs, including smaller ones. By using $\omega_c < 15^\circ$ one would miss the larger facets ($> 60 \mu\text{m}$ in size), that were actually observed at cleavage initiation sites. Furthermore, for $\omega_c > 15^\circ$, the difference in area of larger PCFs is less affected by a further increase in ω_c , if one considers the

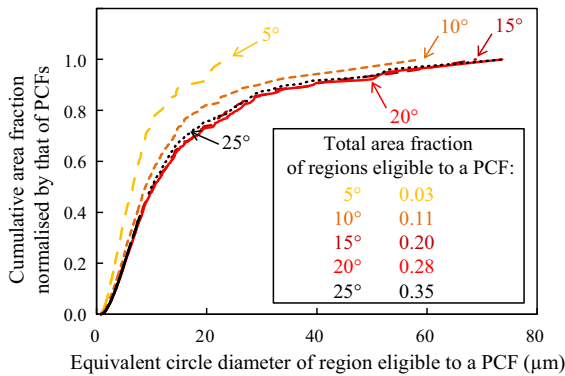


Fig. 8 Effect of critical deviation of $\{001\}$ poles from loading axis, ω_c , on the size distribution of regions that are considered to be sensitive to cleavage cracking (i.e., eligible to a PCF). Steel A, (RD, TD) plane. The total area fraction of such regions is indicated for each value of ω_c

area fractions normalised by the total area of PCFs, i.e., the actual shape of the size distribution (Fig. 8). For $\omega_c = 20^\circ$, the regions covered with PCFs correlated well, both in location and in size, to the ones occupied by larger entities in the microstructure (Fig. 2), as already pointed out by Schofield et al. (1974), yet with no local crystal orientation analysis. The present results indicate that these entities possess a $\{001\}$ plane close to the (RD, TD) plane and that they could favour cleavage fracture along the (RD, TD) plane of Steel A. As a first-order approximation, the value of ω_c was thus set to 20° in the following, i.e., only grains having a $\{100\}$ plane misoriented by less than 20° from the investigated plane were considered as eligible to PCFs.

As stated above, the unit crack path for cleavage fracture is the PCF, and not the individual grain. A PCF is thus a region across which a $\{001\}$ cleavage crack may propagate readily from one grain to the next one, as long as $\{001\}$ planes are not “too strongly” misoriented between the two considered grains. For two neighbouring grains (here, a and b) to belong to the same PCF, (1) their individual values of ω^i should be lower than ω_c and (2) the misorientation angle between the involved $\{001\}$ planes, $\alpha^{a,b}$ (Fig. 7), should not exceed a critical value, α_c .

To get a first insight of the value of α_c , deviation angles between cleavage facets were analysed by quantitative fractography as reported in Tankoua et al. (2014a). A full cleavage fracture surface that presented a large cleavage facet at the initiation site, with no delamination microcrack, was selected for this anal-

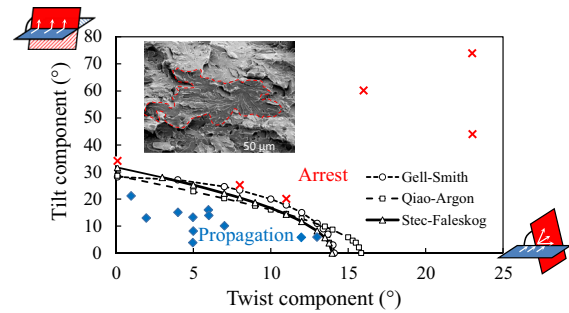


Fig. 9 Quantitative fractography of the cleavage initiation site of a NT specimen of Steel A tested at -100°C along ND (delineated by the dashed line in the inset micrograph): microcrack propagation (full diamonds) versus arrest (full squares) as a function of estimated local tilt and twist components of the deviation. Microcrack propagation is schematized with white arrows in pure tilt and pure twist configurations close to the vertical and to the horizontal axis, respectively. The criteria formulated by Stec and Faleskog (2009), after Gell and Smith (1967), Qiao and Argon (2003) and Stec and Faleskog (2009), and adjusted to the present data are reported with open symbols and dotted, dashed and continuous lines, respectively

ysis, namely, a NT specimen of Steel A tested along ND (inlet in Fig. 9). This first facet was defined as the region containing the crack initiation site, within which a cleavage crack propagated with no strong discontinuity in river pattern and without any ductile tearing of ligaments. The boundary of this facet was delimited by ductile ligaments, separating that facet from misoriented regions where both the fracture surface and the river pattern were oriented in a significantly different way than in that first facet. Crack propagation was supposed to occur readily along the first facet, and to have been hindered at the facet boundary. The local normal direction to the cleavage crack plane was determined in a number of points from the 3D-reconstructed fracture surface.

The conditions of cleavage microcrack propagation versus microcrack arrest were determined as follows, with details reported in the “Appendix”. Let us consider a cleavage crack propagating along given plane, as facet 1 with normal \mathbf{n}_1 and attempting to propagate across an adjacent crystal (cleavage plane with normal \mathbf{n}_2), as illustrated in Fig. 14 in the “Appendix”. Two extreme situations could be encountered, according to the relative orientations of \mathbf{n}_1 , of \mathbf{n}_2 , and of the local tangent to the boundary of the first facet, \mathbf{b} . If both cleavage facet planes contain direction \mathbf{b} , i.e., $\mathbf{b} // \mathbf{n}_1 \times \mathbf{n}_2$, the cleavage crack propagating along facet 1 could tilt

toward the cleavage plane of facet 2, without leaving any unbroken material behind it. This is schematically represented as a “pure tilt deviation” close to the “tilt angle” axis in Fig. 9. If $\mathbf{b} \perp \mathbf{n}_1 \times \mathbf{n}_2$, continuous propagation of a single cleavage crack across the entire boundary segment of orientation \mathbf{b} is not possible. This “pure twist” case is illustrated close to the “twist angle” axis in Fig. 9. To further propagate, the crack has to restart from several locations at the boundary and to leave unbroken ligaments. In the present work, the tilt and twist components of the deviation between neighbouring facets were calculated with in-house software (Andrieu 2013). The values determined within this first cleavage facet give an indication of the deviation angles which could not stop cleavage microcrack propagation along that facet. The values determined across the cleavage facet boundary indicate which deviation angles could strongly hinder or even locally stop cleavage crack propagation. The results are plotted in Fig. 9.

As already denoted in Gell and Smith 1967, Qiao and Argon 2003, Andrieu 2013, and Pineau 2015, for a given misorientation angle, a twist misorientation appears as a more efficient barrier to cleavage crack propagation than a tilt misorientation, because the microcrack has to propagate from one or several points (vs. from the whole boundary in a tilt configuration). Consequently, crack propagation across a twist boundary through a so-called “break-through window” (Lu et al. 2011) locally creates ligaments that have then to be broken, by brittle grain boundary failure in the fully brittle range (Gell and Smith 1967) and, in the ductile-to-brittle transition, by grain boundary shearing (Lu et al. 2010). A tilt angle of up to 20° does not hinder crack propagation; this observation is in agreement with previous findings on bainitic microstructures (see e.g. Gourgues et al. 2000; Lambert-Perlade et al. 2004). For mixed (tilt + twist) misorientations, a twist angle as low as 10° appeared to be sufficiently high to arrest the first cleavage microcrack (corresponding tilt angles being yet also high for these particular measurements).

Experimental measurements were further compared in Fig. 9 with predictions from existing models, derived from experiments on Fe–3Si alloys. The first model was proposed by Gell and Smith (1967) and based on the energy release rate from crack propagation into the second grain. The second model was proposed by Qiao and Argon (2003) and based on the work required to create additional, tilted cleavage fracture surfaces and to

fracture the grain boundaries by a traction-separation phenomenon. The third model was proposed by Stec and Faleskog (2009) based on finite element computational analysis of crack propagation across a grain boundary that was represented by cohesive elements. For these three models, the formulation by Stec and Faleskog (2009) was adopted and the ratio between the critical grain size for given tilt and twist angles to that for zero-misorientation was adjusted to 1.13, 1.30, and 1.215 for the Gell–Smith, the Qiao–Argon, and the Stec–Faleskog models, respectively. The hypotheses underlying these models do not take into account the elastic-plastic anisotropy of individual grains that may greatly affect the values of local stress intensity factors. In addition, the amount of experimental data was low, especially for high-twist, low-tilt boundaries. Nevertheless, the qualitative agreement between experimental measurements and the shape of predicted curves appeared very satisfactory.

In the present work, and based on this preliminary analysis, a critical misorientation angle between $\{001\}$ planes, α_c , not higher than 20° was considered a suitable criterion for the definition of potential cleavage facets, since cleavage propagation might not be stopped for deviation angles lower than that value.

Any accurate determination of α_c would involve a large number of measurements of deviation angles between individual cleavage facets, here considered as $\{001\}$ planes. EBSD data processing procedures have recently been reported to automatically extract values of $\alpha^{a,b}$ from EBSD maps (Ghosh et al. 2016a,b) but were not available in the present case. As only a limited amount of data was provided by quantitative fractography, the value of α_c could not be accurately determined. A simpler, readily-available estimate, well-suited to analyse large data sets, was chosen instead. The misorientation angle $\beta^{a,b}$ between neighbouring grains a and b (and not between their $\{001\}$ planes, see Fig. 7), was used. It was thought to be correlated to the misorientation between cleavage planes. As a consequence, the critical value used for $\beta^{a,b}$ to define a PCF, β_c , was considered as a first, simplified estimate for the definition of PCFs, to be used to compare microtextures along various planes of the plate.

To derive a value of β_c , the boundaries of PCFs determined with various values of β_c were compared to those of larger entities (Fig. 2). The best agreement was

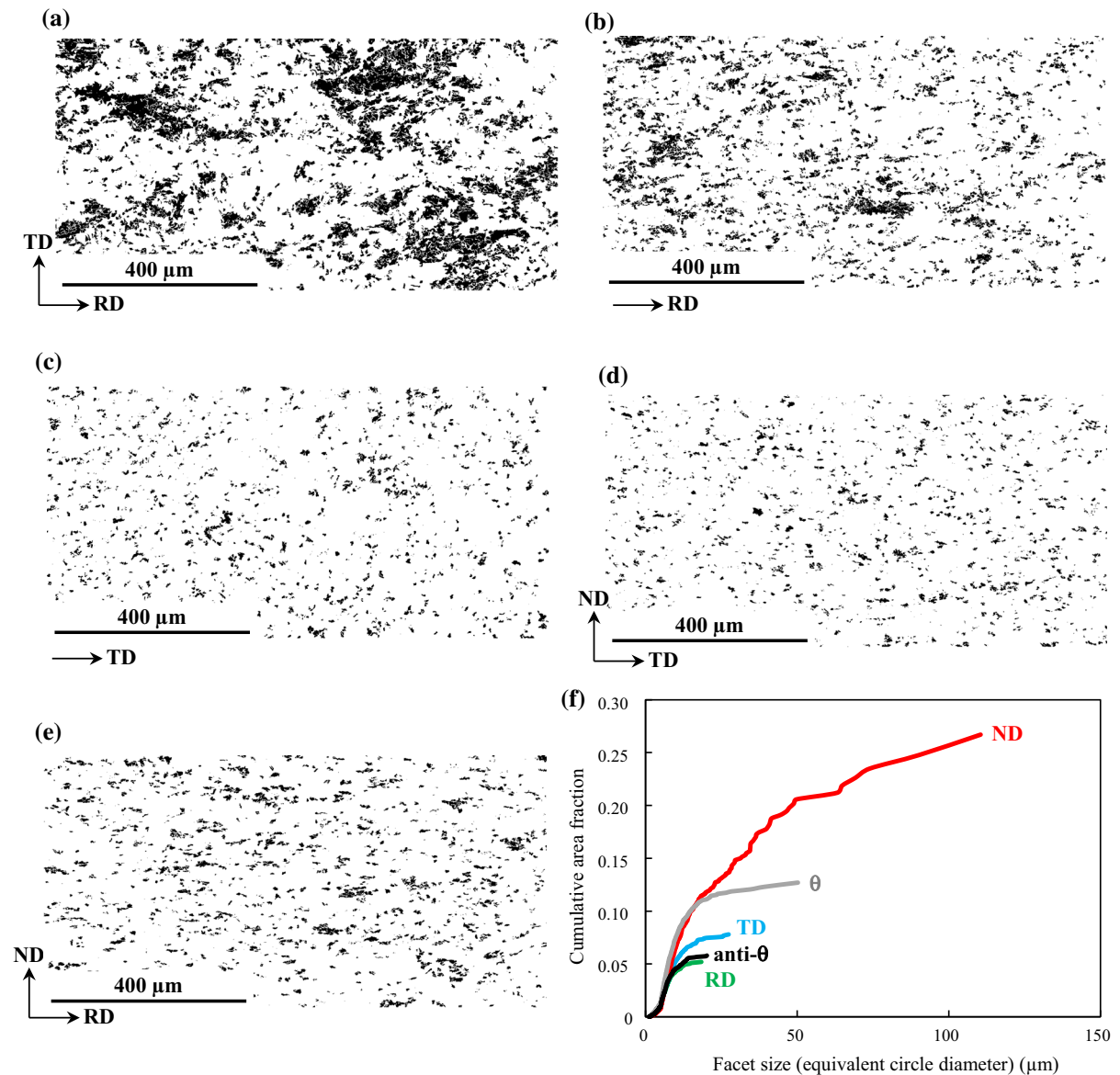


Fig. 10 Microtexture quantification of the sensitivity to $\{001\}$ cleavage cracking of Steel A by EBSD mapping of PCFs (black regions) along **a** (RD, TD) planes; **b** θ -planes; **c** anti- θ -planes;

d (TD, ND) planes; **e** (RD, ND) planes. **f** Size distribution of PCFs ($\omega_c = 20^\circ$, $\beta_c = 10^\circ$); the area fraction is normalised by the total investigated area (not only that of PCFs)

obtained for $\beta_c = 10^\circ$ so that this value was adopted for the microtexture analysis.

The values of $\omega_c = 20^\circ$ and $\beta_c = 10^\circ$ were then assumed to also be relevant for Steel B and for the other investigated planes since (1) the microstructures of both steels were similar to each other and (2) from fracture surface observations, the physical mechanisms of cleavage fracture appeared to be the same.

3.4.2 Quantification of the microstructural anisotropy relevant to cleavage fracture

The spatial and size distribution of PCFs obtained from the planes of interest in Steels A and B are shown in Figs. 10 and 11, respectively. The average fraction of PCFs is indicated in Table 4. Even if the morphology of individual grains was almost isotropic and the gross tex-

ture was not highly pronounced, the strong microtexture anisotropy of Steel A was clearly evidenced. Large PCFs were found in the (RD, TD) plane (Fig. 10a); from individual orientation measurements, these large PCF belonged to the slight rotated cube texture component in that steel. In the θ -plane, PCFs were smaller and elongated along RD (Fig. 10b). In the other planes (Fig. 10c–e), PCFs were even smaller and equiaxed. In particular, the θ -plane and anti- θ -plane strongly differed in the spatial and size distribution of PCFs. The spatial distribution of PCFs in the (RD, TD) plane appeared very heterogeneous, even over typical distances up to 500 μm . Consequently, sampling effects still might have affected the quantification of microtexture in that plane.

The anisotropy in microtexture of Steel B differed from that of Steel A. The θ -plane exhibited a high area fraction and number density of PCFs, homogeneously distributed in the plane (Fig. 11b). The (RD, TD) plane contained smaller PCFs (Fig. 11a), that appear to be less homogeneously distributed than along the θ -plane. The other three planes showed much smaller PCFs (Fig. 11c–e).

For both steels, individual PCFs in the (RD, ND) and θ -planes appeared somewhat elongated along RD. This suggests that the thermomechanical rolling process also introduced a *local* anisotropy in microtexture, in addition to the anisotropy at the larger scale evidenced from EBSD maps.

4 Discussion

4.1 Origin of brittle tilted fracture during BDWTT

The analysis of BTF during BDWTT of hot-rolled steels should take a number of physical phenomena into account, namely, any anisotropy in plastic flow that could affect the stress normal to the θ -plane, any anisotropy in microtexture that could affect the sensitivity to brittle cleavage fracture along θ -planes, as well as dynamic loading effects associated to wave propagation.

The rather low anisotropy in flow stress, as well as the fact that BDWTT specimens tested along RD–TD never exhibited BTF, tend to show that BTF is rather due to a microstructural anisotropy than to a purely mechanical phenomenon. In a companion study of the same steels, fracture toughness tests evidenced BTF for

TD–RD compact tension specimens (Tankoua 2015). As such, the contribution of dynamic loading is not a first-order phenomenon. On the other hand, the microtexture of both steels exhibited a small size and rather low area fraction of PCFs in the anti- θ plane of both Steels A and B, compared to that in both the θ -plane, the rolling plane and the plane of flat cleavage fracture (i.e., the RD, ND plane for TD–RD impact test specimens). As a consequence, BTF in these specimens seems mainly due to the anisotropy in microtexture of both steels, rather than to the anisotropy in mechanical properties or to any dynamic loading effect intrinsic to impact tests.

In many instances, BTF in BDWTT specimens was accompanied by delamination cracks that could be attributed to the rather high sensitivity of the (RD, TD) plane of both steels to cleavage fracture, also associated to the size distribution and area fraction of PCFs along those planes (Figs. 10a, 11a). To further investigate the role of delamination in triggering BTF, a few additional BDWTT tests were carried out along TD for Steel B to get better understanding of the competition between brittle fracture mechanisms along different planes in a given specimen. In these tests, crack propagation was interrupted using a ballistic method by providing a total energy lower than the energy required for complete fracture. Since the height of the hammer above the specimen was fixed, the impact energy was reduced by decreasing the weight of the hammer from 985 kg down to 430 kg. Three specimens were tested at -60°C , which was the fracture appearance transition temperature (50% shear area) of Steel B. After the tests, two of these unbroken specimens were heated for 1 h at 300°C to obtain colour tinting of the fracture surface. Non-destructive evaluations (NDE) with ultrasonic waves and magnetic-particle inspection allowed for locating macroscopic cracks inside the specimens. Compact tension specimens were then machined from the three BDWTT specimens embedding the detected cracks, and finally broken at room temperature with a load ratio of 0.1 and a frequency of 40 Hz, so that the fatigue crack could be easily distinguished from the cracks generated during the BDWTT.

The tinted zone corresponded to ductile slant and contained delamination cracks (Fig. 12). About 10 mm ahead of the ductile slant, one delamination crack at mid thickness could be observed. This delamination crack did not appear from fatigue post-cracking, since according to observations carried out in the present

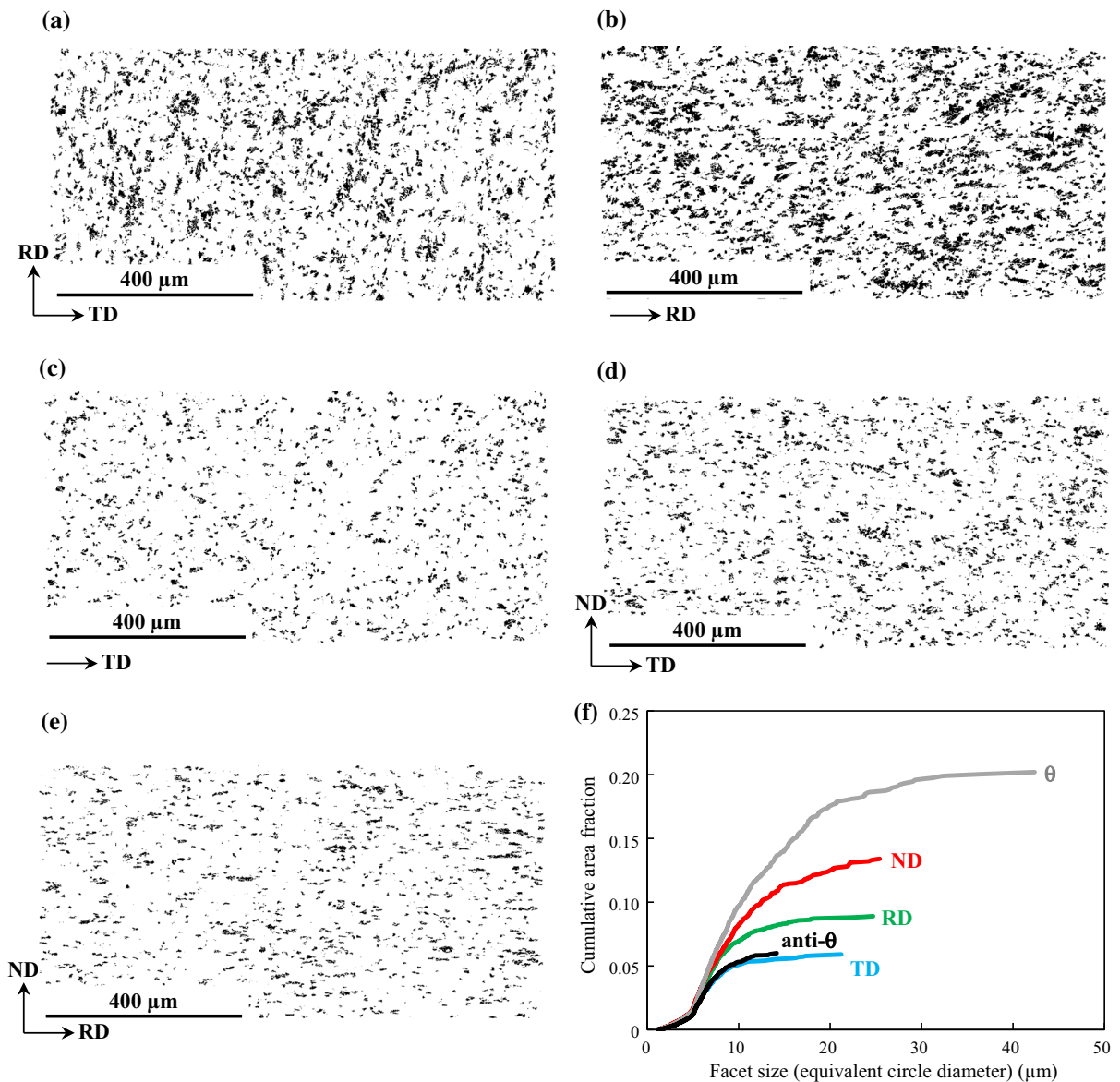


Fig. 11 Microtexture quantification of the sensitivity to $\{001\}$ cleavage cracking of Steel B by EBSD mapping of PCFs (black regions) along **a** (RD, TD) planes; **b** θ -planes; **c** anti- θ -planes;

d (TD, ND) planes; **e** (RD, ND) planes. **f** Size distribution of PCFs ($\omega_c = 20^\circ$, $\beta_c = 10^\circ$); the area fraction is normalised by the total investigated area (not only that of PCFs)

work, delamination never appeared at room temperature. This delamination crack most probably formed during the BDWTT test itself, well ahead of the ductile crack and before the appearance of BTF. As such, BTF should not be considered as an isolated phenomenon, but in close interaction with delamination cracking. This was confirmed by the fact that even in NT specimens, delamination was frequently observed at the ori-

gin of brittle cleavage fracture, especially for specimens tested along the θ -direction at temperatures higher than -196°C (Tankoua 2015). In summary, BTF may be attributed to the high sensitivity of the θ -plane to cleavage fracture, and also possibly to the sensitivity of the investigated steels to delamination, both phenomena being due to their anisotropic microtexture induced by their particular hot rolling processing route.

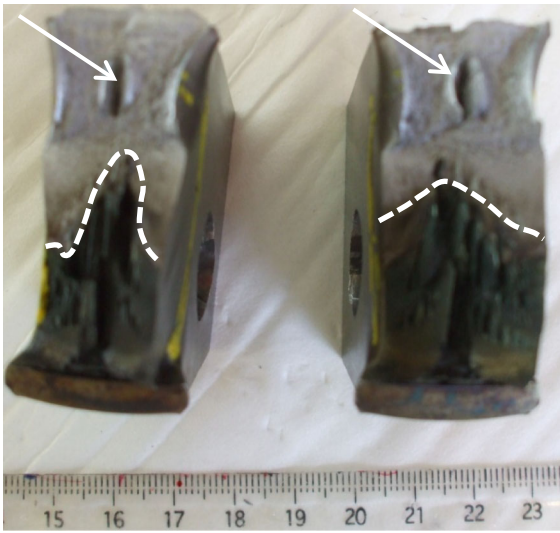


Fig. 12 Macroscopic views of compact tension specimens machined after interrupted BDWTT (Steel B, -60°C), then fatigue fractured at room temperature. The dashed lines delineate the boundary of the tint etched regions; delamination cracks ahead of the tint etched regions are indicated by arrows

4.2 Quantitative link between microtexture and sensitivity to cleavage fracture

In order to quantify the link between anisotropy in microtexture and anisotropy in sensitivity to cleavage cracking, a Griffith-inspired approach was tentatively applied to compare the values of σ_{c-s}^d to those derived from the PCF size distribution. A simple, deterministic approach was chosen instead of a probabilistic fracture model such as e.g. that of Beremin (1983), in order to limit the extent of the experimental database necessary to identify the model parameters. An effective crack size, related to an effective PCF size normal to given loading direction d of Steel S ($S = \text{Steel A or Steel B}$), PCF_{eff-s}^d , had thus to be determined. From fracture surface observations at crack initiation sites, larger facets were more detrimental than smaller ones. The value of PCF_{eff-s}^d should thus take the tail of the size distribution into account. On the other hand, even if large-scale EBSD maps were used, sampling effects cannot be ruled out from experimental PCF size distributions. Consequently, any criterion based on the few larger PCFs (e.g. in the RD, TD plane of Steel A) might induce significant uncertainty on the values of PCF_{eff-s}^d . A simpler, more robust criterion was thus adopted. First, the threshold value to select the so-called

“tail” of the size distribution was set to $8\ \mu\text{m}$, i.e., close to the maximum in the PCF size histograms (steepest part of curves in Figs. 10f, 11f). In fact, a difference of less than 10% in PCF_{eff-s}^d was observed by taking threshold values in the range $8\text{--}12\ \mu\text{m}$. Then, the average area of all PCFs belonging to the tail was calculated, and its equivalent circle diameter was taken as an estimate of PCF_{eff-s}^d . As shown in Table 4 and Fig. 8, the values of PCF_{eff-s}^d were much lower than the size of the first cleavage facet, so that they should only be used in a comparative way.

In classical models using the local approach to cleavage fracture, the critical cleavage stress was inversely proportional to the square root of the size of the first microcrack (Griffith-inspired criterion). In our case, this size was tentatively chosen as PCF_{eff-s}^d . The critical cleavage fracture stress estimated from the Griffith-inspired approach, σ_{G-s}^d , was then estimated using the best fit of parameters C and D of the following equation 5, i.e., a linear fit of the σ_{G-s}^d versus $(PCF_{eff-s}^d)^{-0.5}$ data points:

$$\sigma_{G-s}^d = C + D(PCF_{eff-s}^d)^{-0.5} \quad (5)$$

Note that in contrast to the original Griffith model, a constant C is introduced here, so that no effective surface energy could be readily calculated using the value of parameter D .

Only data points associated to reliable critical cleavage stress values obtained under similar testing conditions (no delamination at initiation site, testing temperature -196°C) were taken into account in the calibration of C and D parameters. Therefore, critical cleavage stresses associated to directions ND, RD and TD for Steel A and TD for Steel B were not used to calibrate the parameters of Eq. (5). The values of C and D were respectively adjusted to ($-1790\ \text{MPa}$), and to $13,740\ \text{MPa}\ \mu\text{m}^{0.5}$. Rather good agreement (maximum discrepancy of $75\ \text{MPa}$) was obtained between that fit and the values used to identify parameters C and D . Using the same equation, the values of σ_{G-s}^d estimated from effective PCF sizes, PCF_{eff-s}^d were then compared to the ones actually estimated from mechanical analysis of the NT tests, σ_{c-s}^d , for all available plane orientations (Table 4 and Fig. 13). The critical cleavage stress estimated along ND for Steel A, σ_{G-A}^{ND} , is considerably lower than σ_{c-A}^{ND} . The fact that σ_{c-A}^{ND} was obtained after large strains at -100°C might play a role in this discrepancy. The uncertainty related to the

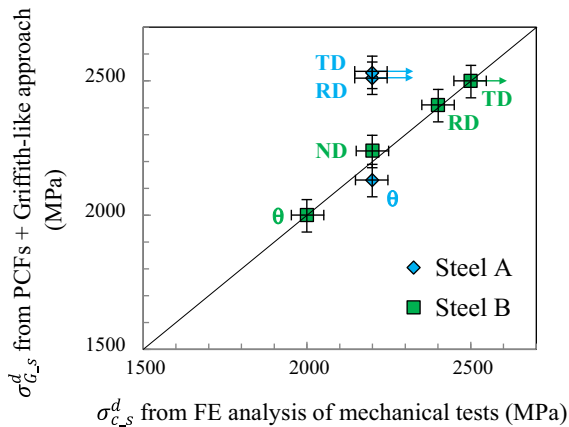


Fig. 13 Comparison between the critical cleavage fracture stresses determined at liquid nitrogen temperature, using FE analysis of tensile tests on notched specimens, with those estimated from quantitative analysis of the microtexture using the concept of PCFs. Arrows indicate that only lower bounds could be estimated, due to the presence of delamination cracks at the origin of cleavage

evaluation of $PCF_{eff_s}^d$ and to any statistical effects resulting from sampling of PCFs might still affect the correlation shown in Fig. 13.

One must notice that the concept of PCF is neither related to the microstructure at the size of individual grains, nor to the macroscopic (average) texture, but to the distribution of *clusters* of unfavourably oriented grains, i.e., to the microtexture itself. In the present case, the strongly anisotropic microtexture at the scale of clusters of grains, inherited from the TMCP process governed anisotropy both in plastic flow and in sensitivity to brittle cleavage cracking. To the authors' knowledge, the simple model set up in this study is the first attempt to quantitatively relate the anisotropic sensitivity to cleavage fracture to the microtexture and plastic flow anisotropy induced by hot rolling in this grade of pipeline steels.

4.3 Linking critical cleavage fracture stresses to the occurrence of BTF during impact testing

Tensile tests on crack-free NT specimens enabled determination of critical stresses triggering unstable cleavage fracture from a single cleavage facet, as a function of the loading direction. The obtained values depend on the population of PCFs within the considered plane. During loading of the BDWTT specimens, BTF will

occur once crack propagation has already started by delamination or prior ductile slant, as shown by interrupted tests (Sect. 4.1). Obviously, the stress state at the crack front of a BDWTT specimen strongly differs from that in a crack-free NT specimen. Nevertheless, in both cases, BTF will only occur if the local opening stress applied to the θ -plane reaches a critical value. The NT specimen methodology allowed investigating the link between that critical value and the microstructure. The same applies for the occurrence of brittle cleavage delamination in front of a ductile propagating crack in BDWTT specimens. The more sensitive the microstructure to cleavage fracture along those planes (as determined using NT specimens), the more sensitive the BDWTT specimens to unstable out-of-plane cleavage fracture.

The origin of BTF both involves the microtexture and the mechanical loading. The microtexture is responsible for the anisotropy in critical cleavage stress and of the intrinsic sensitivity to cleavage fracture of the θ -plane, at least in an undeformed state. The mechanical loading induces a local opening stress across the θ -plane, which could be affected by the presence of delamination or flat cracks. The local opening stress across the θ -plane evolves during the loading, and BTF is triggered once it reaches a critical value, namely, the cleavage fracture stress of that plane. BTF seems to be mainly controlled by microtexture anisotropy, because BDWTT specimens tested along RD did not exhibit BTF. For these specimens, due to the low anisotropy in strength, the loading conditions are similar to those of tests along TD. The main difference is that the BTF plane is no longer the θ -plane but the anti- θ -plane which appears less sensitive to cleavage fracture (low area fraction and size of PCFs). In a Charpy specimen, despite the occurrence of delamination, the short length of the ligament might not allow the critical local stress for BTF to be reached at the tip of the delamination or ductile crack.

In the present work, the anisotropy in cleavage fracture sensitivity was investigated in the fully brittle fracture domain, with fracture occurring after a small amount of strain. The only exception was for Steel A tested along ND at -100°C , for which the fracture occurred in a largely strained material (see Fig. 6a) and the cleavage fracture stress took an unusually low value (1800 MPa, see Table 4). At the onset of BTF, the presence of a delamination or of a flat crack considerably changed the strain state close to the crack tip, i.e., at the

BTF crack initiation site. The effect of high amounts of plastic strain (as prescribed e.g. at the tip of a propagating crack) on the sensitivity to cleavage fracture is currently under investigation in the steels considered during the present work.

5 Conclusions

In the present work, a quantitative link was established for the first time between the critical cleavage fracture stresses, determined along various directions of two hot-rolled pipeline steels by mechanical analysis taking anisotropic plastic flow into account, and the anisotropy in microtexture characterised using EBSD through the concept of potential cleavage facets. The following conclusions could be drawn.

- Brittle tilted fracture occurred in Battelle-type impact specimens in the ductile-to-brittle transition range. It was mainly due to an intrinsic anisotropy in the sensitivity to cleavage cracking along the considered plane, rather than to plastic flow anisotropy or to effects induced by dynamic loading conditions; the ligament of Charpy ISO-V specimens is long enough for delamination to occur, but too short for brittle tilted fracture to be triggered during crack propagation.
- The anisotropy in critical cleavage fracture stress determined in the brittle temperature range from round notched specimens was as high as 25% in the considered steels; a methodology specific to low-thickness plates was successfully developed to obtain this result.
- The high sensitivity to brittle fracture along the rolling plane is linked to a high density of large clusters of crystals that are likely candidates for cleavage facets; a methodology has been set up to readily quantify the size and spatial distribution of these so-called “potential cleavage facets”.
- A Griffith-inspired approach allowed a quantitative link between the anisotropic critical cleavage fracture stress (at $-196\text{ }^{\circ}\text{C}$) and the anisotropic effective size of potential cleavage facets.
- Tight microtexture control during thermal-mechanical controlled processing, at the scale of several ferrite grains, appears as a key point to control the sensitivity of hot-rolled pipeline steels to brittle tilted fracture during impact testing.

Acknowledgements Financial support from the French Agency for Research and Technology (ANRT) under CIFRE Grant No. 2011/1199 is gratefully acknowledged. Fruitful discussions with Dr M. Mazière (MINES ParisTech) and technical help from A. Laurent and A. Meddour (MINES ParisTech) and from Frank Rootsart, Martin Liebeherr, Andries De Geest and Nuria Sanchez (OCAS) are gratefully acknowledged.

Compliance with ethical standards

Conflict of interest The authors declare that they have no conflict of interest.

Appendix: Determination of the tilt and twist components of a cleavage crack deviation to cross a cleavage facet boundary

Let us consider a first facet with normal \mathbf{n}_1 that has been created by a cleavage crack. The local orientation of the facet boundary is \mathbf{b} . Let us consider that the closest possible crack propagation plane in the adjacent grain has normal \mathbf{n}_2 . In the general case, \mathbf{b} is neither parallel (pure tilt) nor perpendicular (pure twist) to the cross-product $\mathbf{n}_1 \times \mathbf{n}_2$. The situation is illustrated in Fig. 14. The orientation of facets 1 and 2 is schematized on both sides of the facet boundary, to better illustrate the calculation procedure.

Let $\mathbf{p} = \mathbf{n}_1 \times \mathbf{b}$ be the direction belonging to facet 1 and perpendicular to boundary \mathbf{b} . The tilt component is calculated in the auxiliary plane P_{tilt} , containing both \mathbf{p} and \mathbf{n}_1 (its normal is direction \mathbf{b}). It is the angle between the so-called \mathbf{ti} direction (belonging to both P_{tilt} and cleavage facet 2: $\mathbf{ti} = \mathbf{n}_2 \times \mathbf{b}$) and direction \mathbf{p} . Mathematically, it is expressed as follows:

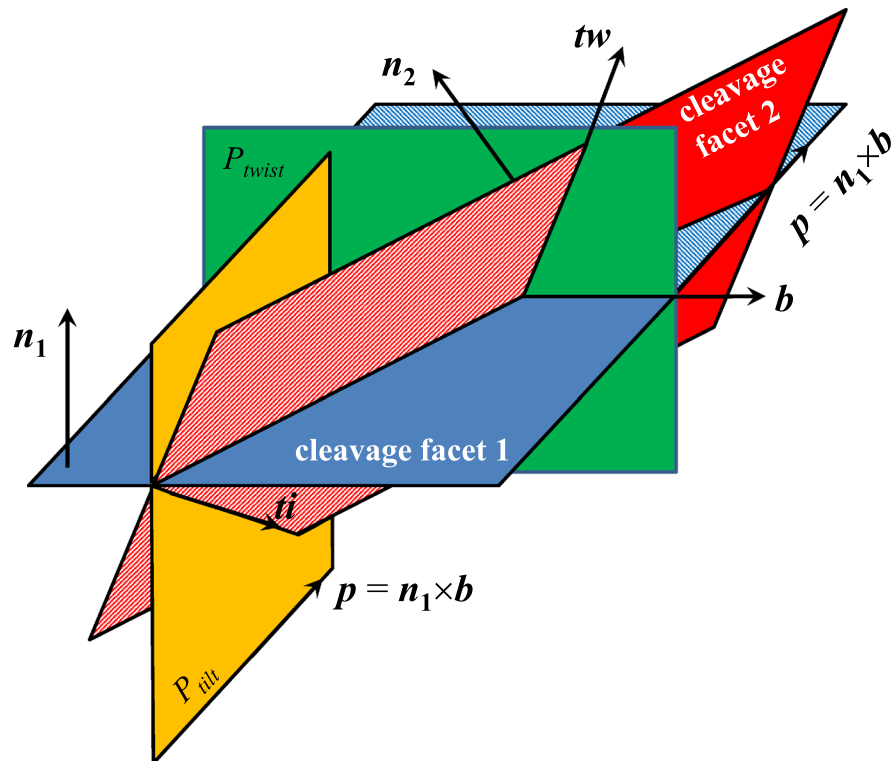
$$\text{tilt_component} = \cos^{-1} \left(\frac{(\mathbf{n}_2 \times \mathbf{b}) \cdot (\mathbf{n}_1 \times \mathbf{b})}{|\mathbf{n}_2 \times \mathbf{b}| \cdot |\mathbf{n}_1 \times \mathbf{b}|} \right) \quad (6)$$

The twist component is calculated in the auxiliary plane P_{twist} , containing both \mathbf{b} and \mathbf{n}_1 (its normal is direction \mathbf{p}). Let \mathbf{tw} be the direction common to both plane P_{twist} and facet 2, i.e., $\mathbf{tw} = \mathbf{p} \times \mathbf{n}_2$, which can be rewritten as $\mathbf{tw} = (\mathbf{n}_1 \times \mathbf{b}) \times \mathbf{n}_2$. The twist component is the angle between \mathbf{tw} and direction \mathbf{b} , mathematically expressed as:

$$\text{twist_component} = \cos^{-1} \left(\frac{((\mathbf{n}_1 \times \mathbf{b}) \times \mathbf{n}_2) \cdot \mathbf{b}}{|(\mathbf{n}_1 \times \mathbf{b}) \times \mathbf{n}_2| \cdot |\mathbf{b}|} \right) \quad (7)$$

The values of tilt and twist components measured from quantitative fractography data are reported in Fig. 9 of the main text.

Fig. 14 Determination of the tilt and twist components of a cleavage crack deviation in the general case, using the normal to each of the cleavage facets (n_1 and n_2) and the local orientation of the boundary of the first facet, b . For clarity, both cleavage facet planes have been represented in full colour in the grain they belong to, and as hatched regions on the other side of the boundary



tilt component: angle between $ti = n_2 \times b$ and $p = n_1 \times b$

twist component: angle between $tw = (n_1 \times b) \times n_2$ and b

References

- Andrieu A (2013) Mechanisms and multi-scale modeling of brittle fracture modifications induced by the thermal ageing of a pressurised water reactor steel. Ph.D. dissertation, MINES ParisTech, France, 2013, in French. <https://pastel.archives-ouvertes.fr/pastel-00957868>. Accessed on 14 Nov 2017
- ANSI/API (1996) RP 5L3 standard, recommended practice for conducting drop-weight tear tests on line pipe. American Petroleum Institute, Washington, 1996
- Baldi G, Buzzichelli G (1978) Critical stress for delamination fracture in HSLA steels. *Met Sci* 12:459–472. <https://doi.org/10.1179/030634578790433332>
- Barlat F, Lege D, Brem B (1991) A six-component yield function for anisotropic materials. *Int J Plast* 7:693–712. [https://doi.org/10.1016/0749-6419\(91\)90052-Z](https://doi.org/10.1016/0749-6419(91)90052-Z)
- Beremin FM (1983) A local criterion for cleavage fracture of a nuclear pressure vessel steel. *Metall Trans* 14A:2277–2287. <https://doi.org/10.1007/BF02663302>
- Besson J, Foerch R (1997) Large scale object-oriented finite element code design. *Comput Methods Appl Mech Eng* 142:165–187. [https://doi.org/10.1016/S0045-7825\(96\)01124-3](https://doi.org/10.1016/S0045-7825(96)01124-3)
- Besson J, Cailletaud G, Chaboche J-L, Forest S (2009) *Nonlinear mechanics of materials*. Springer, Dordrecht ISBN -13: 978-9048133550
- Bourell DL (1983) Cleavage delamination in impact tested warm-rolled steel. *Metall Trans* 14A:2487–2496. <https://doi.org/10.1007/BF02668890>
- Bouyne E, Flower HM, Lindley TC, Pineau A (1998) Use of EBSD to examine microstructure and cracking in a bainitic steel. *Scr Mater* 39:295–300. [https://doi.org/10.1016/S1359-6462\(98\)00170-5](https://doi.org/10.1016/S1359-6462(98)00170-5)
- Bowen P, Druce SG, Knott JF (1986) Effects of microstructure on cleavage fracture in pressure vessel steel. *Acta Metall* 34:1121–1131. [https://doi.org/10.1016/0001-6160\(86\)90222-1](https://doi.org/10.1016/0001-6160(86)90222-1)
- Brozzo P, Buzzichelli G, Mascanzoni A, Mirabile M (1977) Microstructure and cleavage resistance of low-carbon bainitic steels. *Met Sci* 11:123–130. <https://doi.org/10.1179/msc.1977.11.4.123>
- Cosham A, Jones DG, Eiber R, Hopkins P (2009) Don't drop the drop weight tear test. In: Denys R (ed) Pipeline technology conference, 12–14 Oct 2009, Ostend, Belgium, paper no. Ostend2009-090
- Di Shino A, Guarnaschelli C (2010) Microstructure and cleavage resistance of high strength steels. *Mater Sci Forum* 638–642:3188–3193. <https://doi.org/10.4028/www.scientific.net/MSF.638-642.3188>

- EN (2013) EN10208 standard (replaced by NF EN ISO 3183 standard issued in March, 2013), petroleum and natural gas industries—steel pipe for pipeline transportation systems. International Organization for Standardization (ISO), Geneva, Switzerland
- Fujishiro T, Hara T (2011) Effect of separation on ductile crack propagation behavior during drop weight tear test. In: Chung JS, Hong SY, Langen I, Prinsenber SJ (eds) Proceedings of the twenty-first international offshore and polar engineering conference. The International Society of Offshore and Polar Engineers (ISOPE), Cupertino, pp 237–242
- Gell M, Smith E (1967) The propagation of cracks through grain boundaries in polycrystalline 3% silicon-iron. *Acta Metall* 15:253–258. [https://doi.org/10.1016/0001-6160\(67\)90200-3](https://doi.org/10.1016/0001-6160(67)90200-3)
- Gervasyev A, Carretero Olalla V, Pyshmintsev I, Struin A, Arabey A, Petrov RH, Kestens LAI (2013) X-80 pipeline steel characteristics defining the resistance to ductile fracture propagation. In: Denys R (ed) Sixth international pipeline technology conference, October 2013, Ostend, Belgium, Soete Laboratory, Gent, Belgium. ISBN: 9780957531024, paper number S19-02. <http://hdl.handle.net/1854/LU-5866094>
- Gervasyev A, Carretero Olalla V, Sidor J, Sanchez Mouriño N, Kestens LAI, Petrov RH (2016a) An approach to microstructure quantification in terms of impact properties of HSLA pipeline steels. *Mater Sci Eng A* 677:163–170. <https://doi.org/10.1016/j.msea.2016.09.043>
- Gervasyev A, Petrov R, Pyshmintsev I, Struin A, Leis B (2016b) Mechanical properties anisotropy in X80 line pipes. In: International pipeline conference, vol 3, September 2016, Calgary, Canada. ISBN: 978-0-7918-5027-5, paper number IPC2016-64695. <https://doi.org/10.1115/IPC2016-64695>
- Ghosh A, Modak P, Dutta R, Chakrabarti D (2016a) Effect of MnS inclusion and crystallographic texture on anisotropy in Charpy impact toughness of low carbon ferritic steel. *Mater Sci Eng A* 654:298–308. <https://doi.org/10.1016/j.msea.2015.12.047>
- Ghosh A, Patra S, Chatterjee A, Chakrabarti D (2016b) Effect of local crystallographic texture on the fissure formation during Charpy impact testing of low-carbon steel. *Metall Mater Trans* 47A:2755–2772. <https://doi.org/10.1007/s11661-016-3458-y>
- Gourgues AF, Flower HM, Lindley TC (2000) Electron backscattering diffraction study of acicular ferrite, bainite and martensite steel microstructures. *Mater Sci Technol* 16:26–40. <https://doi.org/10.1179/026708300773002636>
- Hara T, Shinohara Y, Asahi H, Terada Y (2006) Effects of microstructure and texture on DWTT properties for high strength line pipe steels. In: Proceedings of ASME international pipeline conference, vol 3, September 2006, Calgary, Canada, pp 245–250. ISBN: 0-7918-4263-0, <https://doi.org/10.1115/IPC2006-10255>
- Hara T, Shinohara Y, Terada Y, Asahi H (2008) DWTT properties for high strength line pipe steels. In: Jin HW, Wang Y-Y and Lillig DB (eds) Proceedings of the eighteenth international offshore and polar engineering conference, Vancouver, BC, Canada, July 2008. The International Society of Offshore and Polar Engineers (ISOPE), Cupertino, pp 189–193
- Hill R (1950) The mathematical theory of plasticity. Clarendon Press, Oxford
- Hong S, Shin SY, Lee S, Kim NJ (2011) Effects of specimen thickness and notch shape on fracture modes in the drop weight tear test of API X70 and X80 linepipe steels. *Metall Mater Trans* 42A:2619–2632. <https://doi.org/10.1007/s11661-011-0697-9>
- Hwang B, Lee S, Kim YM, Kim NJ, Yoo JW, Woo CS (2004) Analysis of abnormal fracture occurring during drop-weight tear test of high-toughness line-pipe steel. *Mater Sci Eng A* 368:18–27. <https://doi.org/10.1016/j.msea.2003.09.075>
- Joo MS, Suh D-W, Bae JH, Bhadeshia HKDH (2012) Role of delamination and crystallography on anisotropy of Charpy toughness in API-X80 steel. *Mater Sci Eng A* 546:314–322. <https://doi.org/10.1016/j.msea.2012.03.079>
- Kotrechko S, Stetsenko N, Shevchenko S (2004) Effect of texture smearing on the anisotropy of cleavage-stress of metals and alloys. *Theor Appl Fract Mech* 42:89–98. <https://doi.org/10.1016/j.tafmec.2004.06.007>
- Lambert-Perlade A, Gourgues AF, Besson J, Sturel T, Pineau A (2004) Mechanisms and modeling of cleavage fracture in simulated heat-affected zone microstructures of a high-strength low alloy steel. *Metall Mater Trans* 35A:1039–1053. <https://doi.org/10.1007/s11661-004-1007-6>
- León García O, Petrov R, Bae J-H, Kestens L, Kang KB (2007) Microstructure-texture related toughness anisotropy of API-X80 pipeline steel. *Adv Mater Res* 15–17:240–245. <https://doi.org/10.4028/www.scientific.net/AMR.15-17.840>
- Lu W, Chen J, Chakravarthula SS, Qiao Y (2010) Resistance to cleavage cracking and subsequent shearing of high-angle grain boundary. *Eng Fract Mech* 77:768–775. <https://doi.org/10.1016/j.engfracmech.2009.12.009>
- Lu W, Chen J, Kong X, Chakravarthula SS, Qiao Y (2011) Nonuniform cleavage cracking across persistent grain boundary. *Mech Mater* 43:567–573. <https://doi.org/10.1016/j.mechmat.2011.07.001>
- McRobie DE, Knott JF (1985) Effects of strain and strain aging on fracture toughness of C–Mn weld metal. *Mater Sci Technol* 1:357–365. <https://doi.org/10.1179/mst.1985.1.5.357>
- Mintz B, Morrison WB (2007) Influence of fissures on tensile and fracture toughness of steels with ferrite/pearlite microstructures. *Mater Sci Technol* 23:1346–1356. <https://doi.org/10.1179/174328407X168801>
- Pineau A (2015) Crossing grain boundaries in metals by slip bands, cleavage and fatigue cracks. *Philos Trans R Soc Lond Ser A* 373(2014):0131. <https://doi.org/10.1098/rsta.2014.0131>
- Punch R, Strangwood M, Davis C (2012) Origin and propagation of splits in high-strength low-alloy strip steel. *Metall Mater Trans* 43A:4622–4632. <https://doi.org/10.1007/s11661-012-1307-1>
- Qiao Y, Argon AS (2003) Cleavage cracking resistance of high angle grain boundaries in Fe–3%Si alloy. *Mech Mater* 35:313–331. [https://doi.org/10.1016/S0167-6636\(02\)00284-3](https://doi.org/10.1016/S0167-6636(02)00284-3)
- Ritchie RO, Knott JF, Rice JR (1973) On the relationship between critical tensile stress and fracture and toughness in mild steel. *J Mech Phys Solids* 21:395–410. [https://doi.org/10.1016/0022-5096\(73\)90008-2](https://doi.org/10.1016/0022-5096(73)90008-2)

- Rosenfield AR, Shetty DK, Skidmore AJ (1983) Fractographic observations of cleavage initiation in the ductile-brittle transition region of a reactor-pressure-vessel steel. *Metall Trans* 14A:1934–1937. <https://doi.org/10.1007/BF02645567>
- Sanchez Mouriño N, Petrov R, Bae J-H, Kim K, Kestens LAI (2010) Texture dependent mechanical anisotropy of X890 pipeline steel. *Adv Eng Mater* 12:973–980. <https://doi.org/10.1002/adem.201000065>
- Schofield R, Rowntree G, Sarma NV, Weiner RT (1974) ‘Arrowhead’ fractures in controlled-rolled pipeline steels. *Met Technol* 1:325–331. <https://doi.org/10.1179/030716974803288112>
- Stec M, Faleskog J (2009) Micromechanical modeling of grain boundary resistance to cleavage crack propagation in ferritic steels. *Int J Fract* 160:151–167. <https://doi.org/10.1007/s10704-009-9415-7>
- Sun J, Boyd JD (2000) Effect of thermomechanical processing on anisotropy of cleavage fracture stress in microalloyed linepipe steel. *Int J Press Vessel Pip* 77:369–377. [https://doi.org/10.1016/S0308-0161\(00\)00038-7](https://doi.org/10.1016/S0308-0161(00)00038-7)
- Sung HK, Sohn SS, Shina SY, Lee S, Kim NJ, Chon SH, Yoo JY (2012) Effects of finish rolling temperature on inverse fracture occurring during drop weight tear test of API X80 pipeline steels. *Mater Sci Eng A* 541:181–189. <https://doi.org/10.1016/j.msea.2012.02.019>
- Tankoua F (2015) Ductile to brittle transition in pipeline steels: quantitative investigation of brittle out-of-plane cracking and correlation to microtexture anisotropy. Ph.D. dissertation, MINES ParisTech, France, 2015 (in English). <https://pastel.archives-ouvertes.fr/tel-01212488>. Accessed on 14 Nov 2017
- Tankoua F, Crépin J, Thibaux P, Arafin M, Cooreman S, Gourgues A-F (2014a) Delamination of pipeline steels: determination of an anisotropic cleavage criterion. *Mech Ind* 15:45–50. <https://doi.org/10.1051/meca/2014001>
- Tankoua F, Crépin J, Thibaux P, Cooreman S, Gourgues A-F (2014b) Quantitative investigation of brittle out-of-plane fracture in X70 pipeline steels. *Proced Mater Eng* 3:1149–1154. <https://doi.org/10.1016/j.mspro.2014.06.187>
- Wilkowski GM, Maxey WA, Eiber RJ (1980) Use of the DWTT energy for predicting ductile fracture behavior in controlled-rolled steel pipes. *Can Metall Q* 10:59–77. <https://doi.org/10.1179/cm.1980.19.1.59>
- Yang Z, Kim C-B, Feng Y, Cho C (2008) Abnormal fracture appearance in drop-weight tear test specimens of pipeline steel. *Mater Sci Eng A* 483–484:239–241. <https://doi.org/10.1016/j.msea.2006.09.182>
- Zong C, Zhu G, Mao W (2013) Effect of crystallographic texture on the anisotropy of Charpy impact behavior in pipeline steel. *Mater Sci Eng A* 563:1–7. <https://doi.org/10.1016/j.msea.2012.11.055>

Publisher’s Note Springer Nature remains neutral with regard to jurisdictional claims in published maps and institutional affiliations.